

Review

# A Review of Icing Research and Development of Icing Mitigation Techniques for Fixed-Wing UAVs

Liang Zhou <sup>1</sup> , Xian Yi <sup>1,2,\*</sup> and Qinglin Liu <sup>1</sup>

<sup>1</sup> Key Laboratory of Icing and Anti/De-Icing, China Aerodynamics Research and Development Center, Mianyang 621000, China; zlandtyt@163.com (L.Z.); aseity670@126.com (Q.L.)

<sup>2</sup> National Key Laboratory of Aerodynamics Science and Technology for Aerospace Flight, China Aerodynamics Research and Development Center, Mianyang 621000, China

\* Correspondence: yixian@cardc.cn; Tel.: +86-15892611314

**Abstract:** With the continuous expansion of Unmanned Aerial Vehicle (UAV) applications, the threat of icing on UAV flights has garnered increased attention. Understanding the icing principles and developing anti-icing technologies for unmanned aircraft is a crucial step in mitigating the icing threat. However, existing research indicates that changes in Reynolds numbers have a significant impact on the physics of ice accretion. Icing studies on aircraft operating at high Reynolds numbers cannot be directly applied to unmanned aircraft, and mature anti-icing/deicing techniques for manned aircraft cannot be directly utilized for UAVs. This paper firstly provides a comprehensive overview of research on icing for fixed-wing UAVs, including various methods to study unmanned aircraft icing and the identified characteristics of icing on unmanned aircraft. Secondly, this paper focuses on discussing UAV anti-icing/deicing techniques, including those currently applied and under development, and examines the advantages and disadvantages of these techniques. Finally, the paper presents some recommendations regarding UAV icing research and the development of anti-icing/deicing techniques.

**Keywords:** atmospheric icing; UAV; Reynolds number; aerodynamic penalties; ice mitigation techniques



**Citation:** Zhou, L.; Yi, X.; Liu, Q. A Review of Icing Research and Development of Icing Mitigation Techniques for Fixed-Wing UAVs. *Drones* **2023**, *7*, 709. <https://doi.org/10.3390/drones7120709>

Academic Editors: Tomasz Nowakowski, Artur Kierzkowski, Agnieszka A. Tubis, Franciszek Restel, Tomasz Kisiel, Anna Jodejko-Pietruczuk and Mateusz Zajac

Received: 15 November 2023  
Revised: 11 December 2023  
Accepted: 13 December 2023  
Published: 18 December 2023



**Copyright:** © 2023 by the authors. Licensee MDPI, Basel, Switzerland. This article is an open access article distributed under the terms and conditions of the Creative Commons Attribution (CC BY) license (<https://creativecommons.org/licenses/by/4.0/>).

## 1. Introduction

Recently, unmanned aircraft systems have been among the most significant developments in aviation. The Unmanned Aircraft Systems Roadmap 2005–2030 [1] reports that over 250 UAV models are currently produced in 32 countries worldwide. Initially, drones saw military use, undertaking tasks such as aerial combat and military reconnaissance, because they were cost-effective, posed no threat to human life, and offered extended mission times and access to complex locations that manned aircraft could not reach. Predator, Phoenix, and Global Hawk drones have all found military applications. More recently, UAVs have demonstrated lengthy endurance capacity, increased safety, greater intelligence, and flexibility. Together, these qualities can effectively address the drawbacks of unsafe, less efficient, and costlier manual operations. Consequently, UAVs are increasingly being used across civil fields for a range of tasks—such as electricity inspections, disaster assessments, rescue operations, aerial photography and mapping, and logistics and delivery. Notably, during heavy rain floods in China’s Henan Province in July 2021, the fixed-wing UAV “Pterodactyl” provided emergency communication assistance to the affected populace, facilitating emergency relief work in the disaster region [2]. Villeneuve [3] proposed the concept and design of using the GRIFF 135 heavy-lift rotary drone to spray anti-icing fluid on aircraft.

Currently, the drone industry is growing rapidly worldwide, with many countries introducing policies to meet national needs. However, drone icing is becoming a significant issue. Ice accretion on the leading edge of the wing alters the wing geometry and reduces the aerodynamic performance of the UAV, causing reduced lift, increased drag, and a higher

risk of stalling [4]. The potential of flight icing (as seen in Figure 1 [5]) may render UAVs inoperable in icy weather and even result in crashes. During some military operations, 25% of UAVs experienced icing, negatively impacting mission success [6]. Three U.S. Army General Atomics MQ-1 Predator drones crashed due to icing in Afghanistan in 2001 and 2002, and the U.S. Army's Northrop Grumman Global Hawk drone also crashed due to icing during Operation Enduring Freedom in Afghanistan [7].



**Figure 1.** Ice accretion on fixed-wing UAV [5].

To mitigate the flight risk posed to UAVs by icing, current anti-icing strategies include grounding UAVs [8] or modifying their path planning [9]. Military missions, such as those in Kosovo, have suspended the use of Hunter drones from October to April [10], significantly inhibiting their operation in icing conditions. Existing anti-icing/deicing methods used for manned aircraft (e.g., anti-icing liquid, pneumatic type, electric-thermal type, etc.) are not entirely suitable for unmanned aircraft due to their complex structure, large mass, or high energy consumption. There is a need to develop innovative anti-icing/deicing strategies specifically for UAVs to mitigate the risk of icing. The United States, Canada, Russia, China, France, Turkey, and several other countries are developing anti-icing/deicing systems for UAVs, but further research is necessary, given that the application of such technology on UAVs is less developed and less widespread than on airplanes.

## 2. Methods of Studying Ice Accretion on a UAV

Research on icing has primarily focused on manned aircraft, wind turbines, and power lines. It was not until the early 21st century that UAVs garnered attention. Studies on icing in manned aircraft can be traced back to 1940, while research on icing in the domain of UAVs is relatively new and limited [11,12]. The early work on UAV icing, specifically discussed, was published by Siquig in 1990 [11], which is considered the first explicit discussion of UAV icing. With the increasing widespread use of UAVs, there is a growing demand for research in the field of UAV icing.

Compared to manned aircraft, UAVs are more susceptible to ice-related hazards due to three main reasons [13]. Firstly, the troposphere holds most of the water vapor in the atmosphere, experiencing complex airflow and weather phenomena like thunderstorms, fog, and low-temperature clouds. Most drones operate within the troposphere. Icing events for aircraft primarily occur during takeoff and landing phases, whereas many UAVs face the risk of icing throughout their entire flight process. Secondly, the smaller size of UAVs, including their wings and propellers, compared to larger aircraft means that ice of the same thickness has a greater impact on UAVs, increasing the probability of stalling in advance. Thirdly, limited energy resources and the absence of anti-icing/deicing capabilities in most UAVs restrict their ability to prevent icing. The Reynolds number, a crucial distinction

between UAV and manned aircraft icing, is generally lower for UAVs, significantly influencing the icing process. Therefore, conducting research on UAV icing is of vital importance for safe UAV operations and designing effective anti-icing/deicing strategies. The rotation of the propeller of a rotary-wing drone creates additional flow complexity [14], resulting in different icing characteristics compared to fixed-wing drones. Due to limitations in length, this article only introduces research on icing of fixed-wing UAVs.

Experimental studies and numerical simulations are the primary methods employed in UAV icing research.

### 2.1. Experimental Studies

UAV icing tests are carried out mainly through flight and wind tunnel tests.

#### 2.1.1. Flight Tests

Flight tests, the most effective method to obtain relevant data, are limited by test weather conditions, continuous monitoring and hence, are rare.

In 2013, Bottyán [15] performed UAV flight icing tests on two different UAVs (an ELBIT Skylark-I LE short-range UAV and a Northrop Grumman RQ-4 Global Hawk Block 30 high-altitude, long-endurance UAV) in the Carpathian Mountains in order to develop an ice accumulation model. In 2016, Williams et al. [16] used a prefabricated ice-like material glued to the wing of the Kahu-Hawk UAV for aerodynamics and stability tests. In 2017, Matiychuk et al. [17] conducted a natural icing flight test with an M-10-2 “Oko” UAV. The results showed that the leading edge of the wing, the leading edge of the tail, the video antenna, and the airspeed sensor’s front surface were affected by icing. With a thickness of approximately 1.5 mm on the leading edge of the wing, the test showed that icing led to a 40% increase in drag and a 10% increase in energy consumption for drone operation, as per flight recorder analysis. Avery [18] performed three UAV flight tests in 2019 to confirm the icing vulnerability of small UAVs during low-altitude flights. One test revealed ice geometries formed on the UAV’s surface due to the flight flow field, which confirmed the influence of pressure distribution on low-speed ice accretion physics. However, the lack of cloud signature sensors precluded the determination of atmospheric water content. In 2021, Siddique [19] conducted tests on the Sky Hunter fixed-wing UAV in three different weather conditions: windy, calm, and icy. Glaze ice was noticeable on the leading edge of the wing, while overflow water could be observed on the wing surface. The propeller was covered with a thick layer of ice. In comparison to calm wind conditions, the UAV experienced a significant increase in power consumption by approximately 240% during icy weather, resulting in a higher demand on battery power. In 2023, Han et al. [20] conducted a flight test to examine the characteristics of in-flight icing and its impact on fixed-wing UAV flight performance. During the flight, extensive ice structures were observed on almost all exposed surfaces of the UAV, such as the wings, body, stabilizers, pitot tubes, and propellers, with water backflow observed on the wing surface, as shown in Figure 2. When completing the same flight task, the power consumption during icing conditions was over 80% higher than when flying under normal non-icing weather conditions.

#### 2.1.2. Lab Tests

A wind tunnel is an experimental device that artificially creates and controls airflow to simulate gas flow around an entity, observe physical phenomena, and measure the effect of airflow. It is a valuable tool for aerodynamic experiments and integral to vehicle research.

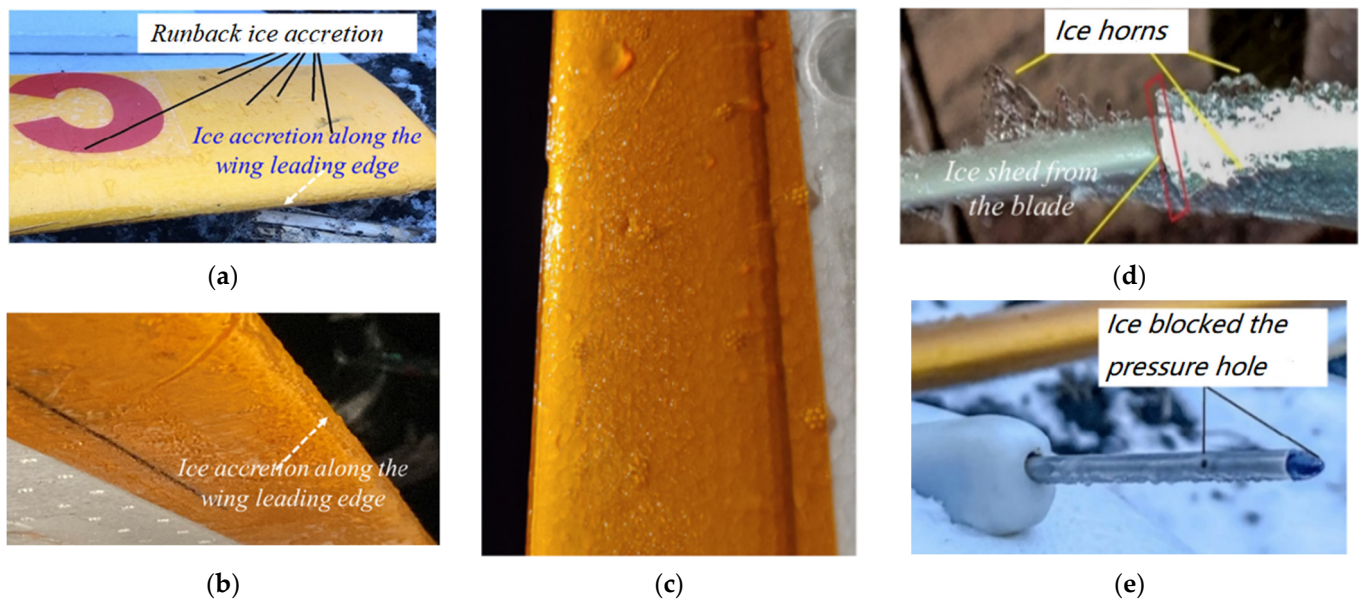


**Figure 2.** Snapshot images of the ice structures accreted on the UAV airframe surface ((a) wing upper surface; (b) wing lower surface; (c) vertical stabilizer; (d) propeller blade; (e) Pitot probe) acquired right after the UAV landed on the ground [20].

Avery and Jacob [21] conducted icing tests of cylinders at low Reynolds numbers in a cryogenic wind tunnel, comparing experimental and numerical results. Williams et al. [16] investigated the RG-15 airfoil in the NRC Altitude Icing Wind Tunnel in 2017. Oswald et al. [22] conducted an experimental study using 3D printed glaze shapes to analyze the icing performance of a medium-sized fixed-wing UAV with the RG-15 airfoil at the largest wind tunnel facility in the Karmen Institute, Belgium. The glaze shapes were derived from previous icing wind tunnel experiments, with their 2D profiles shown in Figure 3. Finally, the experimental results were compared with the FENSAP numerical results.

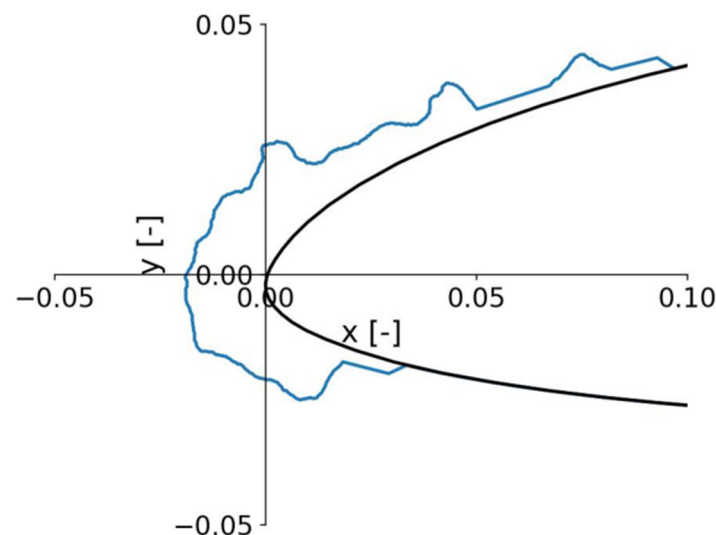


**Figure 3.** A 2D icing profile obtained from the experiment [22]. The blue line represents the ice shape, and the black line represents the clean airfoil.

Hann carried out three main experimental campaigns to gather ice shape data for UAV wings at low Reynolds numbers. In spring 2019, Hann [23] conducted experiments at the Cranfield icing wind tunnel on the RG-15 and NREL S826 airfoils. These tests yielded three

different icing patterns: glaze, mixed, and rime ice, with Reynolds numbers around  $10^5$ . In fall 2019, Hann et al. [24,25] performed additional icing studies on the RG15 airfoil at the VTT icing wind tunnel facility in Finland, focusing on glaze and mixed ice conditions. In 2020, Hann expanded the experimental study to the NREL S826 airfoil, conducted at the Norwegian University of Science and Technology wind tunnel, investigating three different icing conditions: glaze, mixed, and rime ice [26]. Li et al. [27] examined the dynamic ice accumulation and unsteady heat transfer processes of NACA0012 airfoils of thermoplastic materials and aluminum, respectively, under the same icing conditions in the icing research wind tunnel at Iowa State University.

## 2.2. Numerical Studies

Improved computer processing power and new computational fluid dynamics techniques have made numerical simulations a cost-effective and efficient way to study ice. Some countries have developed mature icing simulation software [28–30], including LEWICE in the United States, ONERA Icing Code in France, FENSAP-ICE in Canada, and so on. However, these existing icing simulation tools are validated for manned aviation under high Reynolds numbers [23], and further validation is needed to apply them for UAV icing simulation under low Reynolds numbers [31]. In order to better simulate the icing and anti-icing processes of UAVs, researchers have adopted two approaches; one is to verify the effectiveness of existing simulation tools and choose the more suitable one; the other is to develop new models.

### 2.2.1. Validation of Existing Simulation Tools

Hann [32] compared the panel-based LEWICE method to a modern CFD icing code, FENSAP-ICE. Both codes were used to generate three characteristic 2D ice shapes (rime, glaze, and mixed) at low Reynolds numbers on a NREL S826 wing. Figure 4 presents the simulation results for both codes. Rime results were the most similar, with both codes calculating a good match in the extent, direction, area, and overall shape of the ice, although three differences could be detected. Glaze and mixed ice results showed significant differences between the two icing codes. All three icing conditions in FENSAP-ICE exhibited leading-edge separation, with varying degrees of separation strength, weakest in rime and strongest in mixed ice. As a panel method, LEWICE is not designed to capture separation effects, which may fail to represent critical flow features adversely affecting the prediction of ice shapes. Therefore, LEWICE seems more appropriate for the study of UAV icing and aerodynamic losses under rime conditions.

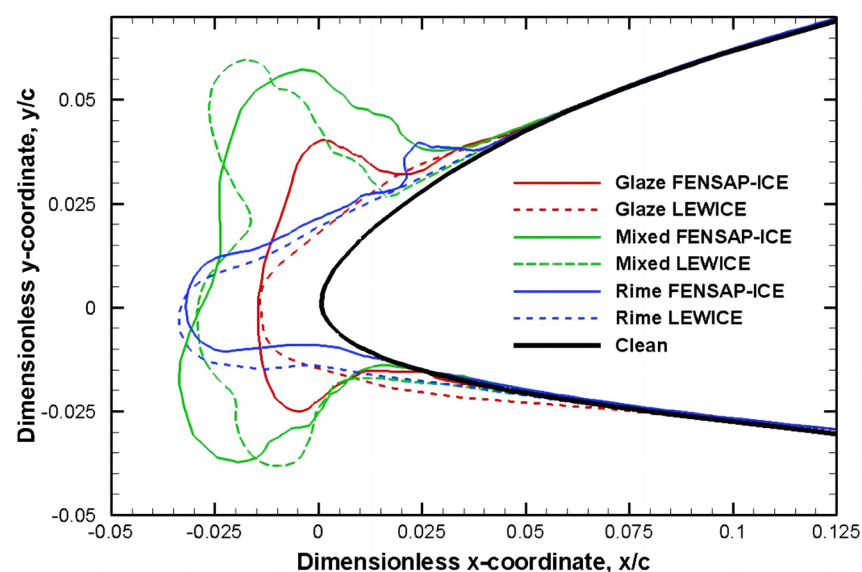


Figure 4. Ice shape results with LEWICE and FENSAP–ICE for the test cases [32].

Yirtici et al. [33] performed numerical icing simulations for three NREL S826 airfoils with different spreading ratios using the XFOIL [34] panel solver. XFOIL predicted larger ice shapes under frost conditions compared to LEWICE. In addition, the XFOIL solver predicted drag coefficients in good agreement with experimental data, but overpredicted lift coefficients in the low angle of attack to the stall region.

Oswald et al. [22] used the FENSAP-ICE flow solver module and the one-equation Spalart-Allmaras (SA) turbulence model for icing simulations of the RG-15 airfoil. The clean RG-15 airfoil was simulated in steady-state 2D RANS CFD with flow transition locations predicted by the software tool XFOIL. Flow transitions were assumed to be triggered by ice accumulation. Simulation parameters are derived from experimental conditions. Comparison of the numerical results with experimental data indicated that the SA turbulence model seemed to be of limited applicability for estimating ice-induced aerodynamic losses at low Reynolds numbers. Other higher-order turbulence models such as Reynolds stress and nonlinear eddy viscosity models should be investigated for numerical simulations.

Hann et al. [26] simulated the aerodynamic losses of the NREL S826 airfoil under icing using SA and Menter's  $k-\omega$  SST turbulence models and compared them with experimental data. The simulations matched well with experimental data for clean and streamlined icing airfoils, but had limitations for complex ice shapes and stall prediction. Experimental stall behavior was not captured by either model. The SA model overpredicted lift values, while the  $k-\omega$  SST model tended to underpredict the maximum lift angle and predict earlier stall.

The flow around UAVs operating at low Reynolds numbers ( $O(10^5)$ ) is mainly laminar, leading to laminar separation bubbles (LSBs) that affect lift, drag, and pitch values. Muhammed and Virk [35] used  $k-\omega$  SST and transitional  $k-\omega$  SST turbulence models to numerically simulate and evaluate their ability to predict LSBs on the RG-15 airfoil at a Reynolds number of  $1.07 \times 10^5$ . The  $k-\omega$  SST turbulence model predicted fully attached flow at lower angles of attack but failed to predict LSBs. On the other hand, the transitional  $k-\omega$  SST turbulence model accurately predicted LSBs but with an earlier separation onset time.

### 2.2.2. Developing of New Models

Bottyán [15] developed an onboard icing estimation method with a simple ice accumulation model to examine the influence of airflow temperature, liquid water content (LWC), wing geometry, and airflow velocity on UAV wing icing.

Szilder and McIlwain [36] investigated the impact of Reynolds number on the icing process by using a morphogenetic icing method to derive an analytical model for UAV icing. The model was combined with a CFD solver (which could predict the Stanton number) and a droplet trajectory solver to simulate ice accretion on the NACA0012 2D airfoil in the Reynolds number range of  $5 \times 10^4$  to  $5 \times 10^6$ . Some of the model's predictions were in close agreement with experimental results.

Avery and Jacob [21] developed a cylindrical volume icing model called ALRIA in Matlab to study UAV icing conditions. The ALRIA model was composed of droplet flow fields and thermal equilibrium sections, including low Reynolds number formulas for cylindrical components in the range of  $Re \sim 3 \times 10^5 - 8 \times 10^5$ . During ALRIA's development, Avery enhanced the earlier work of Langmuir et al. [37] and derived a method to calculate droplet collection efficiency as a function of the stagnation point angle. Avery and Jacob subsequently conducted experiments, model simulations, and LEWICE3D simulations on chosen scenarios to compare their results. As shown in Figure 5, comparative analysis indicated that the ALRIA model was able to simulate ice accretion under dry and most wet icing conditions, but it performed poorly for large and thick ice accretions.

Flight experiments are costly and have limited validation. Numerical icing simulation software and wind tunnel tests have played an important role in solving aviation icing issues and should also be applied to UAV icing. However, there is still not enough work done in this new field. Additionally, existing experimental and numerical results often do

not match, perhaps due to inaccurate simulations or errors in the tests. It is necessary to continue research on UAV icing.

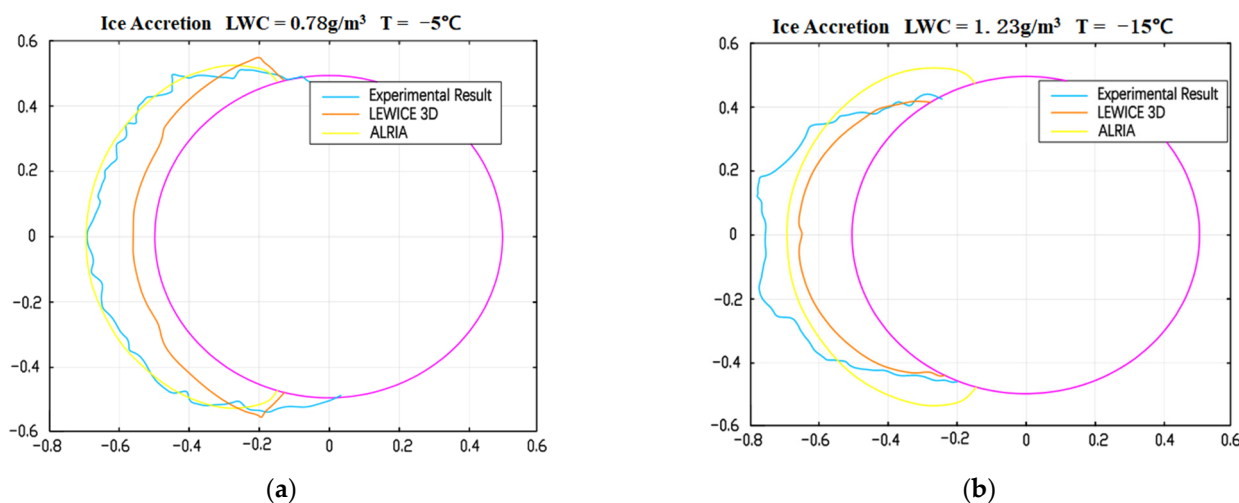


**Figure 5.** Comparison of experimental, model simulation, and LEWICE3D simulation results under given operating conditions: (a)  $-5^{\circ}\text{C}$ ,  $30.5\text{ m/s}$ ,  $0.78\text{ g/m}^3$  for 5 min; (b)  $-15^{\circ}\text{C}$ ,  $30.5\text{ m/s}$ ,  $1.23\text{ g/m}^3$  for 5 min [21]. The pink line represents the cross-section of the cylinder.

### 3. Advances in UAV Icing Research

Like manned aircraft, UAV icing can be affected by conditions such as free stream velocity, atmospheric temperature, LWC, median volume diameter of droplets (MVD), angle of attack, Reynolds number, and so on.

#### 3.1. Typical Icing Characteristics of UAVs

Many of the characteristics of UAV icing are the same as for manned aircraft, as shown below. As the atmospheric temperature decreases, the ice changes from glaze to mixed ice and finally to rime [38]. The mass of ice increases with rising temperature [39]. Changes in the angle of attack cause changes in ice accretion position [16]. Increases in LWC and MVD lead to a greater amount of ice accretion, and the shape of ice shifts from streamlined to angular [38]. When investigating based on the FAR 25 Appendix C icing envelope, ice accretion is a function of temperature, LWC, and MVD. As the MVD value increases, the ice size decreases and eventually disappears due to the decrease in LWC [40]. When the LWC is large, a considerable amount of latent heat must be removed to freeze the impacting droplets completely, which is favorable for glaze. However, as the potential for latent heat removal increases at lower temperatures, the temperature also plays an important role here.

However, most unmanned drones have some typical characteristics in icing, given their differences from manned aircraft, such as lower Reynolds numbers, smaller flight speeds, lower flight altitudes, smaller sizes, and different body materials.

In low Reynolds number flows, a bubble can form at the leading edge of the UAV wing, which can cause laminar-to-turbulent flow transition. Low Reynolds numbers also impact surface heat transfer and supercooled droplet trajectory, which can, in turn, affect the airfoil icing process. Szilder and McIlwain [36] developed an icing analysis model for drones in 2011 to study the effect of Reynolds numbers on icing behavior. With increasing Reynolds numbers, while holding other parameters constant, ice transformed from feathery rime to a combination of glaze and rime and eventually to solely glaze. Flight conditions that resulted in glaze at high Reynolds numbers might result in rime at low Reynolds numbers. Additionally, as the Reynolds number increased, mixed ice conditions tended to occur at colder air temperatures and lower LWCs.

Szilder and McIlwain [36] also compared ice accretion at low and high Reynolds numbers for specific flight distances, which was crucial for understanding actual flight

situations of UAVs. At a specific flight distance, as the Reynolds number increased, the relative ice accretion size significantly decreased while the actual ice mass increased. Low Reynolds numbers are advantageous for rime formation that lowers aerodynamic losses, but it also increases the relative thickness of ice, which raises aerodynamic losses. Therefore, the changes in aerodynamic characteristics during UAV flight are dependent on specific flight conditions.

The Reynolds number is a function of chord length and velocity. Bottyán et al. [15,41] observed in 2013 that when the ambient temperature was  $-4.2\text{ }^{\circ}\text{C}$ , an increase in airspeed from 10 m/s to 130 m/s would cause icing behavior to change from less dangerous dry ice to more dangerous horn ice. In addition, it was observed that the ice accretion rate increases with speed, and the ice accretion thickness also increases with speed. However, the ice thickness at the stagnation point decreases and disappears completely at higher speeds. Hann and Johansen [24] studied the effects of chord length and velocity respectively on UAV icing based on the FENSAP-ICE software. The study revealed that airspeed had progressively increasing effect on rime, mixed, and glaze ice. Increasing airspeed slightly increased the relative ice thickness of rime, enlarged the droplet impact area but does not affect its streamlined ice shape. The impact of airspeed on mixed ice was different. As the airspeed increased, the morphology of mixed ice transitioned from rime-like to glaze-like, resulting in reduced ice thickness and significantly increased ice limit. The impact of airspeed on glaze was similar to that on mixed ice. At lower wind speeds, glaze on the airfoil had a streamlined shape, but it bore less resemblance to rime compared to low-speed mixed ice conditions. At higher speeds, the glaze formation became more complex, and the ice limit significantly increased.

The impact of chord length was consistent across the three types of ice formation, as shown in Figure 6. Firstly, the relative ice thickness significantly increased for smaller wing sections. Secondly, the relative ice limit was significantly increased. Thirdly, there was no significant impact of chord length variation on ice geometry. Greater relative ice thickness often indicates higher aerodynamic losses. This essentially means that unmanned aircraft are much more sensitive to icing than manned aircraft, with icing conditions rated as “trace” or “slight” for manned aircraft potentially being severe for small unmanned aircraft [42].

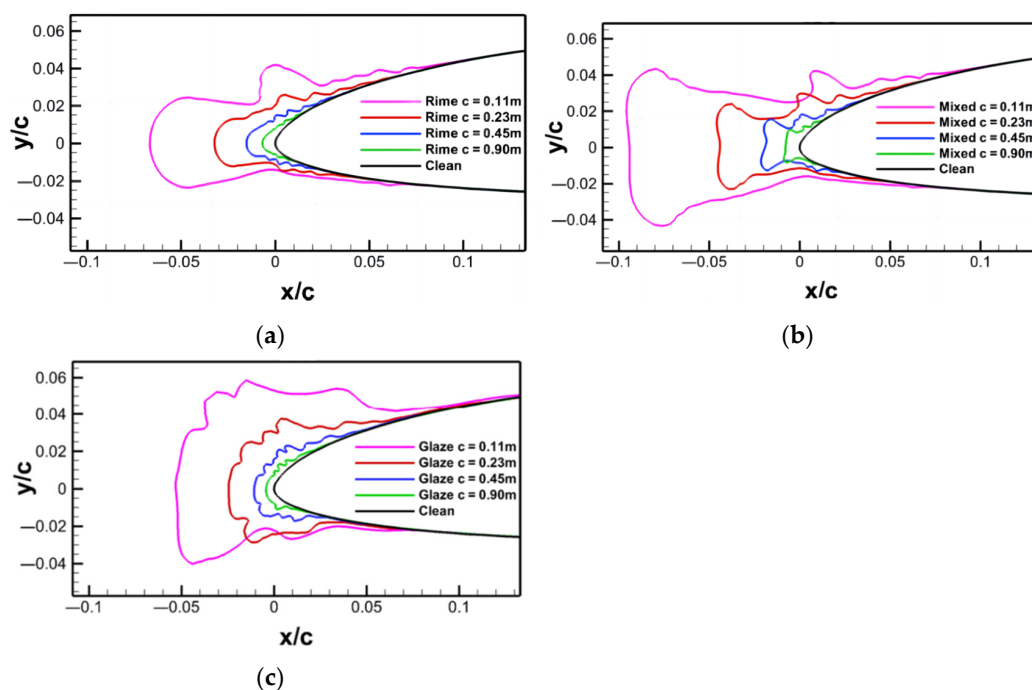


**Figure 6.** Ice shapes for the three meteorological icing conditions rime (a), mixed (b), and glaze (c) for the variation of chord length [24].

Flying altitude affects UAV icing through changes in natural environment, including lower temperature and atmospheric pressure at higher altitudes, varying liquid water content and droplet size. In addition, the body material of drones also plays a role in icing, with thermop materials releasing latent heat from melting much more slowly compared to aluminum. Li [27] found that the surface temperature near the leading edge of the wing of the UAV model using thermoplastic material is higher, the “heating” area is larger, the surface water flow on the wing surface is more obvious, and more complex stream ice structures are formed at downstream positions beyond the direct impact area of supercooled water droplets.

### 3.2. Changes in Aerodynamic Characteristics Caused by Icing

Reynolds number significantly affects the quantity, location, and geometry of ice accumulation, which are closely related to performance losses [4]. In 2007, Cistriani et al. [43] studied the aerodynamic performance of an iced UAV wing in a wind tunnel. Maximum lift was reduced by 30% compared to a clean wing. Hann et al. [44] demonstrated that icing increased drag, decreased lift, and lowered maximum angle of attack. Also, Hann et al. [32] analyzed aerodynamic performance penalties of the NREL S826 wing with rime, glaze, and mixed ice. Overall, mixed ice showed severe performance degradation followed by glaze and rime. Fajt [39], Hann [24], and Oswald [22,45] reported high aerodynamic losses of the RG-15 airfoil in glaze ice conditions, with drag coefficient increasing up to 170%. Szilder and Yuan reported severe aerodynamic losses of the SD7037 airfoil in glaze conditions [46]. Simulation results showed a maximum decrease in lift coefficient of 16%, drag coefficient increasing up to 300%, a 12% decrease in pitch moment, and an early stall at  $9^\circ$  (clean airfoil stalled at  $11^\circ$ ). Hann et al. [26] conducted an analysis on the aerodynamic degradation of the NREL S826 airfoil at different Reynolds numbers during 2020. According to Figure 7, glaze and horn ice formations resulted in the most significant drag loss, with a corresponding 26% loss in lift and up to a 330% increase in drag coefficient at zero angle of attack. This substantial drag increase and changes in lift occurred due to the occurrence of large separation bubbles resulting from the horn geometry. The study found that the geometric shape of ice was the cause of flight performance degradation, with more complex formations causing more severe degradation in performance. The effect of Reynolds number on the results appeared to be relatively small, and higher Reynolds numbers led to greater lift and reduced drag levels.

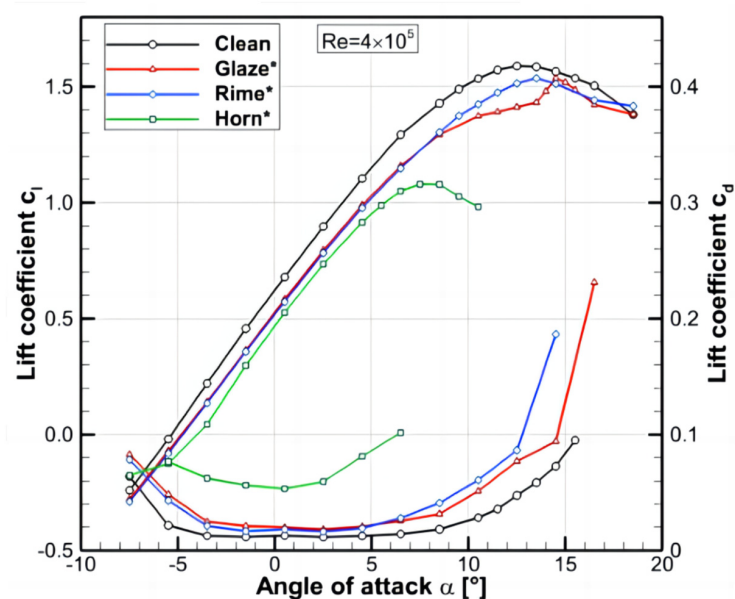


**Figure 7.** Experimental results for lift and drag of the LEWICE ice shapes for  $Re = 4 \times 10^5$  [26]. \* indicates that the ice shape was calculated by LEWICE.

The laminar separation bubble (LSB) depends on the airfoil geometry and flow velocity, and can be observed within the Reynolds number range of  $5 \times 10^4$  to  $3 \times 10^6$  [47]. When formed, the LSB alters the behavior of the boundary layer, transitioning the flow from laminar pre-separation to turbulent post-reattachment. As the angle of attack increases and the separation bubble becomes smaller in length and thickness, the LSB moves upstream [35]. At low Reynolds numbers (defined as  $Re < 10^6$ ), where the boundary layer is thicker and the LSB is larger in size [48], the significance of laminar flow characteristics and LSB becomes even more pronounced. It could potentially impact ice accretion and subsequently degrade aerodynamic performance [48]. Additionally, observations by Oo [49] revealed that flow at low Reynolds numbers experienced delayed reattachment, increased separation, and the possibility of secondary separation bubbles. Such intricate flow patterns at low Reynolds numbers may explain some of the “peculiar” phenomena encountered during UAV flights under icing conditions.

In numerical simulations, icing causes a decrease in lift and an increase in drag across the entire range of angle of attack values [26]. However, certain experiments reveal a sudden increase in lift when the angle of attack reaches a specific value after entering the stall zone. This lift increase could be due to the ice shape acting as a nose-down effect [50] or localized separation bubbles [51]. As Reynolds number decreases, the lower inertia of the boundary layer causes trailing edge separation to occur at a lower angle of attack, resulting in a more significant impact on lift. It explains why this anomalous behavior occurs at all Reynolds numbers, with the most prominent effect observed at low Reynolds numbers. Seifert and Richert [52] observed a lesser lift increase in their experiments. Similar effects at low Reynolds numbers were recorded by Jasinski et al. [53].

Ice-induced separation bubbles (ISBs) represent another type of airflow separation that affects the aerodynamic characteristics of an iced airfoil. ISBs form downstream of ice accretion at the leading edge, with their size increasing along with the angle of attack, while the starting position remains constant. High-frequency oscillations can be observed in the transitional region between ISBs and LSBs [54]. Both Oo [49] and Bragg [4] concluded that ISBs and LSBs exhibit similar characteristics. Oo observed an increase in lift and a decrease in drag for an iced airfoil compared to a clean airfoil (RG-15) under specific icing conditions. The increase in lift can be explained by the previous section. As for the decrease in drag, the authors attribute it to the relatively larger LSBs present on the clean airfoil compared to the ice-induced separation bubbles.

Appendix A summarizes the main findings of the UAV icing study cited in this article. Although research on UAV icing is currently insufficient, limited research progress indicates that icing significantly deteriorates the aerodynamic performance of UAVs, resulting in reduced lift, increased drag, and premature stall. The reduced maximum lift negatively impacts the stability of UAVs, whereas the heightened drag coefficient results in greater power consumption. These penalties in aerodynamic performance are likely to restrict the range and endurance of UAVs, thereby impacting the successful execution of their missions [55]. It further underscores the significance of developing anti-icing/deicing technologies for UAVs.

#### 4. Existing Anti-Icing/Deicing Techniques for UAVs

The ice protection system (IPS) helps to minimize the negative impacts of icing on aircraft. Conventional aircraft deicing methods use coatings, chemicals, heat, and mechanics [56]. Chemical methods mainly utilize liquids, heat methods include gas heating and electric heating, and mechanical methods refer to using force to separate the ice from the substrate, including pneumatic and electric pulse methods. While these techniques are well established for aircraft, they are relatively new when it comes to UAVs [31]. The inherently limited payload and low available energy of UAVs necessitate lightweight and low-energy IPSs. Therefore, the mature anti-icing/deicing techniques used on aircraft cannot be directly applied to UAVs and require further assessment and improvement.

The pneumatic deicing technique [56] utilizes a high-pressure air source to rapidly expand expansion tubes on the wing surface to break up surface ice, which is then carried away by external airflow. This method is systematic and requires high-pressure gas sources, pressure valves, gas pipelines, and actuated expandable tubes, making it only suitable for large aircraft. However, the entire system is relatively heavy and burdensome for UAVs, and there is no available literature on its use for UAV ice protection.

The liquid anti-icing/deicing technique [57,58] utilizes liquid to reduce ice adhesion to aircraft surfaces or lower the freezing point of water on the surface. Although primarily used for ground anti-icing of aircraft, some aircraft carry liquid and have specific spraying devices to apply liquid for anti-icing/deicing during flight. The “weeping wing” system [59] on the RQ-1B drone [60] continuously pumps a deicing liquid film onto the wing, and liquid is also used for anti-icing/deicing on the MQ-9B UAV [61]. However, this method has a restricted effective time and requires significant liquid consumption, which is too heavy for drones. Therefore, the method is not ideal for anti-icing/deicing.

The hot air anti-icing/deicing technique [62] utilizes heated air from the engine to warm aircraft components and prevent icing. This method is well established and predominantly used for large passenger or military transport aircraft. However, UAVs typically rely on electricity as their power source and are incapable of providing a hot air supply. Consequently, this technique is not suitable for UAVs.

Coatings [63–65] primarily aim to reduce the adhesion strength of water or ice to surfaces, making it challenging for ice to form or adhere to the structure’s surface, thus facilitating ice removal. Although coatings are energy-efficient, they cannot completely prevent icing. Their effectiveness is limited to delaying the freezing of water droplets on the coating surface [66,67]. Currently, researchers are striving to combine passive anti-icing techniques like coatings with active anti-icing/deicing methods such as heating to enhance overall anti-icing/deicing performance [68,69].

The electric anti-icing/deicing technique utilizes electric heating elements to convert electrical energy into heat energy. This process warms the aircraft’s skin or components, thus achieving the desired anti-icing/deicing effect [70,71]. Anti-icing and deicing are two different modes of an electric heating system. The anti-icing mode applies continuous heat to the surface of a structure to prevent ice formation and is primarily used for components where ice formation is not allowed. The deicing mode allows ice to accumulate on the surface until a certain amount is reached, and then applies heat to melt it. The electric heating technique is lauded as an effective anti-icing/deicing method due to its high heating efficiency, precise control, and adaptable configuration. The Gulfstream Pilot Operating Handbook [72] suggests that the electric anti-icing system, operating continuously under icing conditions, should maintain a surface temperature of roughly 38 °C–54 °C. Consequently, a high power supply may be needed to satisfy enhanced anti-icing requirements [73,74]. For instance, a typical general aviation aircraft’s anti-icing area, which utilizes a pad heater, is around 0.90 m<sup>2</sup>, and necessitates around 23,250 W/m<sup>2</sup> of energy to attain the anti-icing temperature. This energy requirement is challenging for any aircraft to handle, let alone drones that have limited energy resources for anti-icing/deicing. The Chinese Wing Loong II drone uses an electric anti-icing system on its wings while simultaneously employing anti-icing coatings to decrease power usage [75]. However, with the emergence of fully electric aircraft, the electric anti-icing/deicing system will enter a new era of development.

Electric pulse deicing technique leverages the interaction between the magnetic field generated by the pulse coil circuit and the induced magnetic field of the metal skin surface. The interaction leads to high-frequency skin vibrations that remove ice from the surface [76,77]. Russia employed this technique successfully on IL-76 and IL-86 aircraft. In recent years, the Orion UAV was also equipped with an electric pulse system to manage icing hazards [78]. This system offers low energy consumption and high efficiency but has its limitations. Composite material skins pose a challenge for this technology because of the difficulty in generating induced magnetic fields.

Few anti-icing techniques are available for unmanned aerial vehicles, which face struggles in handling severe icing conditions. Table 1 lists the application and pros and cons of using traditional aircraft anti-icing technologies on UAVs.

**Table 1.** Application of conventional aircraft anti-icing/deicing techniques to UAVs.

Techniques	Pros	Cons	Applications
Pneumatic type	Simple operation and low cost	Large mass, easily damaged pneumatic sleeve	—
Liquid	No energy consumption	Large mass, short effective time	RQ-1B UAV MQ-9B UAV
Hot air	Air source available on aircraft	No air source on drones	—
Coating	No energy consumption	Short effective time	Wing Loong II UAV
Electric type	Good anti-icing/deicing effect and mature system	High energy consumption with overflow ice	Wing Loong II UAV
Electric pulse type	Low energy consumption and good deicing effect	Composite materials are not easy to generate magnetic fields	Orion UAV

## 5. Exploring Ice Mitigation Techniques for UAVs

Given that anti-icing/deicing techniques for drones are not yet sufficiently developed, scientists are actively working on developing ice mitigation techniques that are UAVs.

### 5.1. Airfoil Optimization

It seems that structural optimization offers a solution to minimize ice accretion on UAVs at the source.

Ghisu et al. [79] incorporated icing conditions into the optimization process for a general aviation airfoil. They considered the uncertainty of the ice accretion location and employed an adaptive polynomial chaos method for quantifying the uncertainty. The method computed how airfoil performance varied with the given changes in ice accretion location. The findings indicated that obtaining the optimal lift coefficient configuration came at the expense of a significant negative pitching moment and a 10% increase in drag coefficient in comparison to a clean wing. It is important to note that the ice shape in their optimization process remained fixed rather than occurring naturally from the icing process.

Li et al. [80] conducted a study in which they optimized a supercritical airfoil to consider the effects of icing. Their results demonstrated a 16.5% increase in the maximum lift coefficient for the icing airfoil at a drag coefficient of 3.7 during cruise conditions. However, the optimization process utilized a fixed ice shape and neglected variations in ice shape that corresponded to the airfoil and icing conditions. Dai et al. [81] proposed an objective optimization method to design ice-resistant airfoils, balancing performance between clean and icing conditions. The optimized configuration displayed considerable improvement in icing performance, indicating a 9.95% increase with a maximum lift coefficient of 4.133 during icing conditions.

Li et al. [40] utilized the Radial Basis Function—Enhanced Differential Evolutionary algorithm to perform two rounds of optimization on a specific UAV. In the initial bi-objective optimization, net lift-to-drag ratio and icing stall performance were considered. The results indicated that the optimal “cruise optimal” design improved the maximum lift coefficient for icing conditions by 18% compared to the traditional “icing optimal” design. During the second optimization, fluctuations in atmospheric icing conditions were taken into account since they significantly affect aerodynamic performance. Environmental parameters were regarded as uncertainties, and a Probability Density Function was assumed. To evaluate the maximum lift coefficient due to varying environmental parameters, the Nonintrusive Polynomial Chaos Expansion formula was utilized. Finally, the mean and variance of the resulting maximum lift coefficient were employed as objectives in the collection of data.

Figure 8 showed that the resulting “Polynomial Chaos Expansions optimal” airfoil had improved icing performance, with a 6.7% increase in maximum lift coefficient.

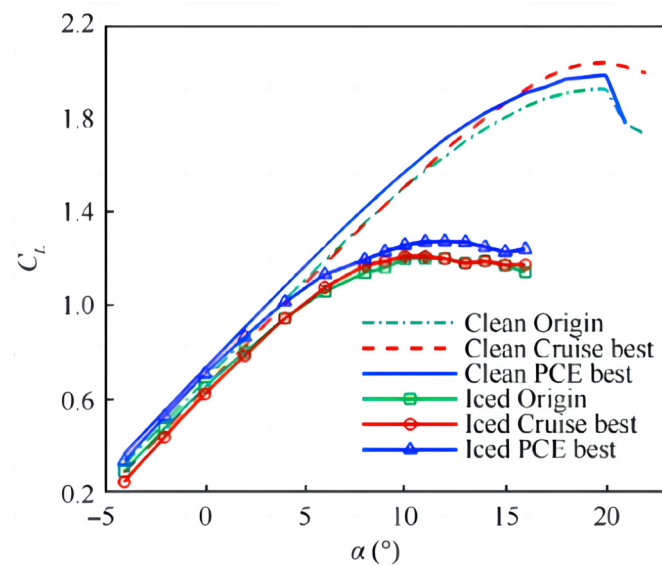


**Figure 8.** Airfoil optimization results [40].

### 5.2. Flight Optimization

Vukit [82] suggested that the most effective approach for avoiding the dangers of natural icing is through precise prediction of conditions that trigger icing and avoiding such conditions. According to several researchers, the weather research and forecasting (WRF) model is capable of accurately predicting meteorological conditions that lead to icing [83]. By combining the WRF model with proxy models [84], a safe envelope or graded safety zones icing in the target area can be generated. This offers crucial data support for optimizing UAV paths.

Narum et al. [85] developed an optimal path planning algorithm for a hybrid electric UAV with an electrical anti-icing/deicing system, using given meteorological forecasts as input data. Particle swarm optimization was used for energy consumption and overall time usage optimization. Multiple simulated datasets were used to test the algorithm. Path planning optimization considering meteorological forecasts for such platforms resulted in a 43% energy efficiency improvement or a 42% flight time reduction between two points, compared to standard straight-line cruising flights.

### 5.3. Coatings

Several methods have been suggested for minimizing ice adhesion, such as “air film isolation” represented by superhydrophobic (SHP) surfaces [86–88], “oil film isolation” represented by slippery liquid-infused porous surfaces (SLIPS) [89–91], and “water film isolation” represented by hydrophilic lubrication layers [92,93] and electrically heated coatings [94,95]. Although coatings have proved to be highly effective for anti-icing purposes, their insufficient durability remains a major drawback.

SHP surfaces have been able to passively reduce interfacial adhesion and promote droplet shedding, demonstrating excellent anti-icing performance. Ye et al. [96] created a hydrophobic coating system composed of fluorinated organic siloxane material for UAV icing protection that exhibited a contact angle  $\theta \geq 115^\circ$  according to experimental measurements. It is important to keep coating thickness within 20 nm to avoid compromising UAV endurance with excess weight. For possible application of SHP surfaces in anti-icing on metallic unmanned aircraft wings, Luo et al. [97] used electrostatic spraying and melt molding processes to make PEEK-PEEK/PTFE/k-SiO<sub>2</sub> composite coatings on the surface of 7075Al alloy, employing PTFE and PEEK as physically blended materials infused with

modified hydrophobic silica ( $k\text{-SiO}_2$ ) particles. The composite coatings exhibited SHP characteristics, retaining excellent mechanical strength even after 51 abrasion cycles and 50 peeling cycles with 3M tape. Moreover, in addition to remarkable self-cleaning properties, water droplets completely froze on the SHP coating at  $-15\text{ }^\circ\text{C}$  within 940 s, which is 43.5 times slower than on a standard 7075Al alloy surface.

The concept of SLIPs, initially introduced by Wong et al. [98], has gained popularity as a passive anti-icing solution. On SLIPs, ice is isolated by a thin oil film retained within the porous structure, which substantially reduces ice adhesion through the “solid-oil-solid contact model”. To demonstrate the potential for anti-icing, Kim et al. [89] developed aluminum-based SLIPs that effectively prevent ice/frost accumulation by facilitating the removal of condensation water and achieving ultra-low ice adhesion. Li et al. [99] combined this surface with electrothermal technology to create a slippery liquid-infused porous electric heating coating (SEHC). Dynamic anti-icing tests revealed that SEHCs reduced energy consumption by 23% compared to dry porous electric heating coatings, and 11% compared to SHC porous heating coatings. Continuous high-speed jetting tests, static deicing/deicing cycles, and dynamic anti-icing tests confirmed that SEHCs exhibit superior durability compared to SHC porous electric heating coatings.

Similar to SHP surfaces and SLIPs, ice on the water-based lubrication layer is also isolated by a water film within the structure. Inspired by ice skating, Chen et al. [92] used dopamine-modified hyaluronic acid to create anti-icing coatings with water-based lubrication layers under mild conditions. Moreover, thanks to the non-selective adhesion property of dopamine, this coating can be used on almost all types of solid surfaces. Dou et al. [93] grafted hydrophilic dihydroxymethyl propionic acid onto a polyurethane substrate to provide hydrophilicity to the coating, which absorbs moisture to isolate ice from the surface. Environmental tests conducted at  $-53\text{ }^\circ\text{C}$  revealed that the water lubrication layer remained intact, and the ice adhesion strength persisted even after 30 deicing and icing cycles, confirming durability. Alternatively, electric heating coatings use Joule heating to melt ice, forming a water film that creates “water film isolation” conditions.

#### 5.4. Electric Heating for Anti-Icing/Deicing

UAVs rely on IPSs that are lightweight and energy-efficient [31]. Electric systems are well suited for unmanned aircraft due to their maturity, nature, and ease of retrofitting onto existing airframes [100]. However, traditional electric heating systems consume a significant amount of energy, which necessitates measures to reduce energy consumption in order to make them suitable for unmanned aircraft. These measures primarily involve selecting materials with improved heating performance, optimizing processes, and implementing more reasonable designs. System optimization often involves a combination of multiple measures.

##### 5.4.1. Selection of High-Quality Materials

Carbon-based materials, such as carbon nanotubes (CNTs) and graphene, which exhibit excellent conductivity and thermal conductivity, are ideal options for utilizing the conductor’s Joule heating effect to de-ice unmanned aircraft [73,101].

In 2013, Buschhorn et al. [73] created a CNT-based IPS that only requires  $1\text{ kW/m}^2$  of power to prevent icing under mild icing conditions. Yao et al. found that a carbon nanotube network/carbon fiber composite structure could effectively de-ice within 15 s at a constant power density of  $4.9\text{ kW/m}^2$  [102]. Zhao developed an electric heating coating by incorporating multi-walled CNTs into polyurethane/paraffin composites, demonstrated a positive temperature coefficient effect, and could automatically control the maximum temperature during heating, thereby protecting the temperature-sensitive composite substrate and saving electricity [101].

In addition, the conductivity of graphene-modified carbon fiber/polyether ether ketone composites was around  $0.1\text{ S/m}$ , resulting in a 35% increase of Joule heating-to-deicing energy conversion efficiency [103]. Glass fiber bundles coated with graphene

displayed low electrical resistance ( $\sim 1.7 \Omega/\text{cm}$ ) and rapid temperature rises (from  $-0.1^\circ\text{C}$  to  $27.3^\circ\text{C}$  within 5 min) when exposed to a 10 V voltage [104].

Cortés et al. discovered that 3D printed circuits utilizing graphene nanosheets and carbon nanotube-reinforced resin are effective for anti-icing purposes [105]. Fluorinated decylated graphene nanoribbon films, a fresh design that merges the low polarizability fluorocarbons and the exceptional electrical conductivity of graphene nanoribbons, are anticipated to offer structural components effective anti-icing/deicing performance [106].

Hexagonal boron nitride is another exceptional heating material due to its high thermal conductivity, superior thermal and chemical stability, and mechanical strength, making it an excellent choice [107]. Since carbon-based materials are capable of shielding electromagnetic waves [108], anti-icing/deicing systems with high radio frequency (RF) transmission rates are necessary to ensure proper functioning of RF equipment, such as radar domes and antennas. In 2020, Hwang et al. proposed an RF transmission heating system for deicing, and its deicing effect was demonstrated by applying a voltage of 40 V to the system at a temperature of  $-20^\circ\text{C}$  [109].

#### 5.4.2. Search for Cost-Effective Manufacturing Processes

The conductivity and thermal properties of carbon fibers allow them to serve as direct heating elements in electric heaters, eliminating the need for separate heating elements. This simplifies the integration of anti-icing/deicing systems into drones, reducing complexity and cost. However, numerous challenges arise from the techniques employed in manufacturing carbon-based heaters, including high costs, energy-intensive processes, limited lifespan, and additional weight on composite materials [110–113]. These factors consequently restrict the applications of carbon-based materials. Consequently, it is imperative to improve manufacturing technology.

Idris [114] employed extrusion printing technology to produce electrical contact points on carbon fibers during the manufacturing of heating devices. The results revealed that the heater was successfully produced, achieving high temperatures suitable for deicing. The proposed carbon fiber heater was estimated to increase costs by only USD  $0.03/\text{cm}^2$ . Vertuccio et al. [110] adopted expanded graphite to create flexible expanded graphite foils through a straightforward and eco-friendly solvent casting process with the addition of PVA. Karim et al. [104] first synthesized scalable amounts of graphene-based ink using the microfluidic exfoliation technique, then utilized the dip-drying solidification coating technique to manufacture highly conductive graphene-based glass fiber yarns. Both techniques are simple, scalable, and extremely suitable for industrial applications. Xu et al. [115] used a casting technique to produce laminated flexible pressure-sensitive adhesive graphene-based composite heaters with exceptional joule heating performance, thermal stability, electrical anisotropy, and mechanical properties. The heater was lightweight and environmentally friendly, enabling it to be used as a custom-shaped flexible deicing heater for various substrates. At a low power of roughly 2.1 W and a bias voltage of 6 V, the heating temperature peaked at  $142.9^\circ\text{C}$ . In addition, the casting method employs simple equipment, has high production efficiency, yields uniform film performance, and is well established in industry.

#### 5.4.3. Design of System Layout

UAVs possess restricted available energy, ensuring the careful design of the electric heating system and minimizing heat for the operating system.

Developed by the Norwegian University of Science and Technology's Autonomous Marine Operations and Systems Center and commercialized by UBIQ Aerospace [100], D•ICE is an electric IPS that implements a heating zone made of carbon fiber. Figure 9b [116] depicts the basic composition of D•ICE, exhibiting a continuously heated special heating zone located at the separation strip by the leading edge of the stagnation point, which is utilized to reduce the energy consumption required for deicing [117]. The strip boosts the aerodynamic force that acts on the ice, enhancing ice removal efficiency. The typical width

of the separation strip is 2–3 mm. Since 2013, D•ICE has been integrated into various styles and sizes of fixed-wing UAVs, then tested in icing wind tunnels and during flight.

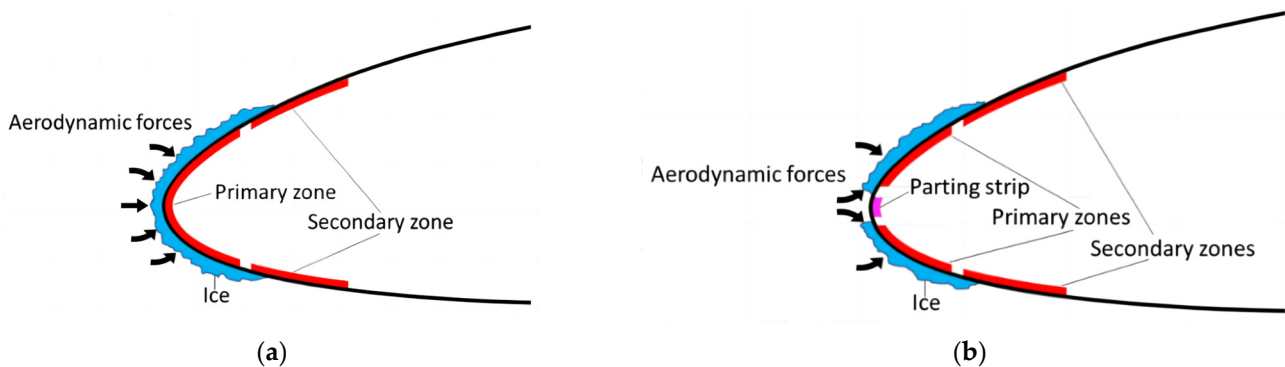


**Figure 9.** Schematic layout of the heating-zones for the (a) conventional deicing and (b) deicing with parting strip [116].

During autumn 2018, D•ICE was tested at the Cranfield icing wind tunnel to identify the minimum heat flux needed to maintain an ice-free surface under two different weather conditions by gradually decreasing the system's power supply [100]. In autumn 2019, the VTT icing wind tunnel facility tested two layouts of the D•ICE system (refer to Figure 9). These experiments were conducted for mid-size fixed-wing UAVs operating at low Reynolds numbers ( $Re = 8\text{--}9 \times 10^5$ ). By adopting separation strips, deicing energy requirements reduced by 50% when compared to traditional deicing systems. For separation strip systems, higher angles of attack resulted in shorter deicing times, reducing such duration by approximately 20–30%.

Roy et al. [118] designed and developed an integrated electrothermal anti-icing system using a thin etched foil heating film. The system was integrated into the leading edge of a CFRP laminate wing of a UAV. Simulated icing flight conditions included an airflow velocity of 102 m/s, an air temperature of  $-6.65\text{ }^\circ\text{C}$ , an MVD of 20  $\mu\text{m}$  for water droplets, an LWC of 0.78  $\text{g}/\text{m}^3$ , and an exposure time of 600 s. The study investigated different IPS heat flux values ranging from 0 to 10  $\text{kW}/\text{m}^2$ . Two IPS designs were considered, one with 5 heating film units and another with 15 units in the leading edge region. The results revealed that the 15 heating film IPS design with a film heat flux of 7.5  $\text{kW}/\text{m}^2$  achieved complete anti-icing functionality, maintaining a wing surface temperature distribution between 0–13  $^\circ\text{C}$ .

Sørensen et al. [119] developed a temperature-controlled anti-icing/deicing system for the airfoil of the X8 Skywalker UAV. The system structure is shown in Figure 10. The core of the system is a coating made of carbon nanomaterials graphene and carbon black, which provides anti-icing functionality. The thermocouple and humidity sensor are responsible for sensing the surface temperature of the airfoil leading edge and the environmental humidity, respectively. Power delivery to the coating is controlled by an Arduino microcontroller based on feedback from the thermocouple and humidity sensor. Different coating layouts were studied within a temperature range of  $-25\text{ }^\circ\text{C}$  to  $+25\text{ }^\circ\text{C}$ . Experiments showed that a layout in which the coating covers the entire length of the wing was preferred, and that the solution was capable of rapidly raising the surface temperature when needed (deicing) and maintaining a roughly constant temperature when needed, while keeping energy consumption within the weight and cost constraints imposed by the small size of the UAV. Sørensen and Johansen [120] investigated the heat flow produced by electric IPS when integrated into small UAVs. The temperature along the heat source was non-uniform under a fixed power supply of 10  $\text{kW}/\text{m}^2$ . The results suggested that utilizing smart methods could be advantageous in reducing power consumption to a minimum.

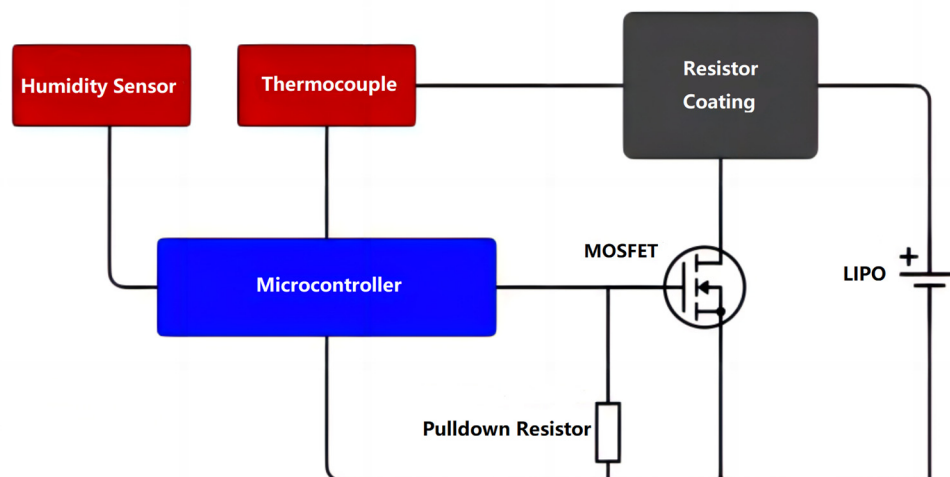


**Figure 10.** Schematic of ice protection system [119].

#### 5.4.4. Combining with Coatings

When compared with traditional anti-icing/deicing systems, hybrid anti-icing/deicing systems that utilize hydrophobic coatings and electric heating systems offer higher energy efficiency, making them ideal for use in UAVs. There has been a significant rise in publications related to hybrid electric systems over the last few decades [121,122].

Zhao [95] employed multi-walled CNTs as heating materials, acrylic resin clear varnish as coating materials, and hydrophobic SiO<sub>2</sub> nanoparticles to create an SHP coating. Anti-icing experiments demonstrated that the multilayer coating not only accomplished low-temperature anti-icing (around 7 °C), but also had efficient electric heating and anti-icing performance. In comparison to conventional electric heating methods, the multilayer coating could reduce anti-icing energy consumption by up to 58%.

Bogoslov et al. [123] developed an integrated electrically heated anti-icing system (IE AIS) that relies on fluorescent film. The IE AIS features a 50 µm fluoroplastic film that functions as a passive anti-icing coating, and a 300 µm thick conductive fluoroplastic film that serves as the heating element. In to these components, the system also includes an electrical current and thermal insulation layer connected to a control system, alongside temperature-sensitive components specifically designed for aircraft parts. By making use of IE AIS, energy necessary for surface deicing could be decreased by 30% as compared to currently available electrically heated anti-icing systems.

Battelle [124] developed a technique that incorporates CNTs into both the barrier and paint layers. When an electric current runs through it, the system acts as a resistive heating coating and creates a highly conductive heating surface. This approach provides several benefits compared to traditional ice-removal systems. Firstly, it is lightweight and requires low power. Secondly, the method utilizes established coating application processes, enabling its direct application to the UAV fuselage.

Yan et al. [125] proposed an anti-icing solution that adds a surface insulation layer, metal heating layer, and bottom insulation layer under a biomimetic anti-icing structural layer to obtain a hybrid anti-icing skin. The biomimetic anti-icing layer, inspired by Qinling giant bamboo, is a multilayer non-uniform high and nanoscale structure. The metal heating layer is made of constantan, which has high resistivity and thermal conductivity and good ductility and bendability. Flight tests demonstrated the excellent performance of this hybrid anti-icing system.

Zhu [126] created a low-energy SHP electric heating anti-icing skin for a UAV by combining a polyimide SHP surface with an electric heating film. Figure 11a shows the production process. In order to optimize the energy utilization of the anti-icing skin, electric wire structures were designed for different regions of the airfoil model to generate differing power densities. The overall design, including the size and regions of the SHC electric

heating skin, is depicted in Figure 11b. Region I, located at the front of the upper wing surface, is 90 mm long and responsible for anti-icing/deicing. Region II is 30 mm long and covers the leading edge of the wing, acting as a hot knife and requiring higher power density than the upper and lower wing surfaces. Region III, 40 mm long, is responsible for anti-icing/deicing the bottom of the wing. Anti-icing wind tunnel experiments demonstrated significant benefits for the SHC electric heating skin over ordinary electric heating skins, with reductions in energy consumption of 52%, 68.8%, and 89.9%, respectively, during three different icing conditions. Test conditions were very similar to those at the University of Quebec [70], with their anti-icing skin yielding reductions of just 13.3% and 34.2%, making the results from Zhu better than those from the University of Quebec.

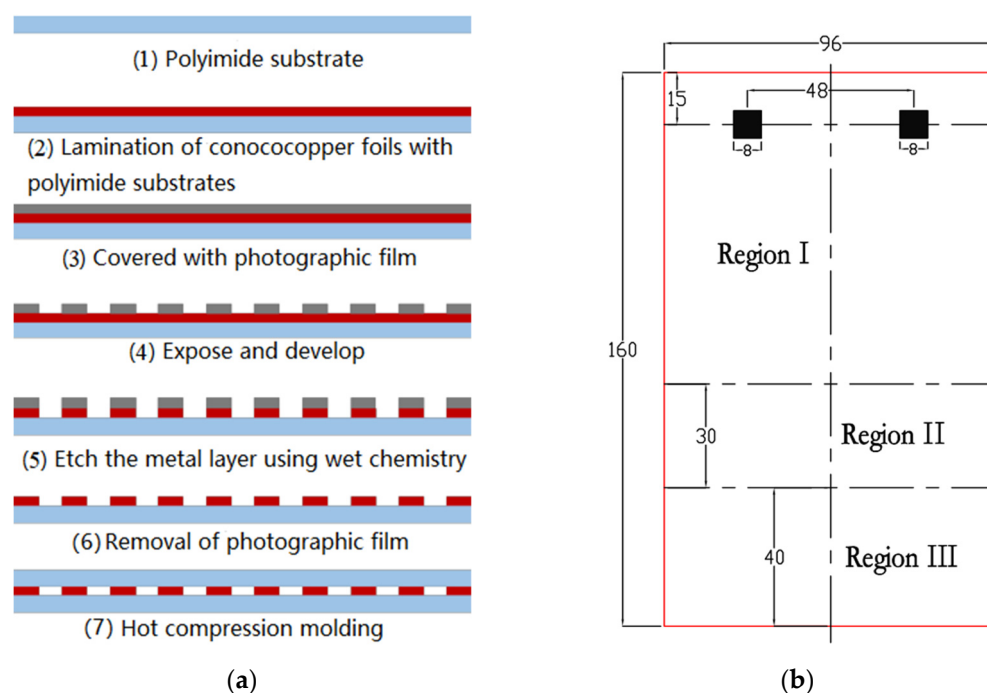


**Figure 11.** Electric heating skin's (a) production process and (b) overall size [126].

### 5.5. Piezoelectric Deicing

The piezoelectric deicing technique has also been developed for aviation [127]. When the current flows in one direction, the piezoelectric crystal bends. Thus, there are two ways for piezoelectric materials to achieve deicing: one is when high-frequency AC is applied to piezoelectric actuators [128], the substrate vibrates at a very high frequency, and the stress generated destroys the ice and substrate; the other is to let the piezoelectric substance work in the low-frequency band and excite the resonant frequency of the structure [129]. Piezoelectric systems have the advantages of small volume, light weight, arbitrary shape, and low energy consumption [130,131], but piezoelectric materials are prone to fatigue and have a relatively short service life. Overall, the piezoelectric technique is a promising deicing method.

Palacios [132,133] utilized piezoelectric patches to generate ultrasonic shear stress at high frequencies, studied the combination of hydrophobic coatings with ultrasonic deicing systems [134], and designed a piezoelectric deicing system [135] effective in promoting shedding ice layers ranging from 1.4 to 7.1 mm thick and under different icing conditions. Budinger [136] compared a ceramic deicing system with Langevin prestressed piezoelectric transducers to find an interesting compromise solution for an ultrasound-based piezoelectric deicing device.

Meanwhile, Venna et al. [129,137–139] used piezoelectric ceramics to excite low-frequency modes (below 1000 Hz) while Struggle et al. [140] performed similar experiments

which proved successful deicing at 307 Hz. Villeneuve [128] designed a low-frequency piezoelectric deicing system for thinned Bell 206 main rotor blades and Bell 206 tail rotor blades, and demonstrated its deicing performance in an icing wind tunnel. For all structures, the power input of the actuator was less than  $19 \text{ kW/m}^2$ . Palanque [141] developed an electromechanical resonance deicing system based on low-frequency piezoelectric actuators, and proved that the prototype had an effective deicing performance with low peak power consumption (less than  $10 \text{ kW/m}^2$ ) and fast deicing.

Surface acoustic wave (SAW) deicing employs piezoelectric material and shows promise as a deicing method due to its ability to provide localized heating, on-site control low power consumption, and system integration. It is achieved by applying high-frequency electrical signals to patterned interdigit electrodes on a piezoelectric substrate, which generates surface vibrations via the reverse piezoelectric effect [142,143]. Heat generation results from both the Joule heating of the interdigitated electrodes and the dielectric losses in the piezoelectric substrate [144,145]. The sketch of the SAW-induced melting process of glaze ice aggregates is shown in Figure 12 [146].

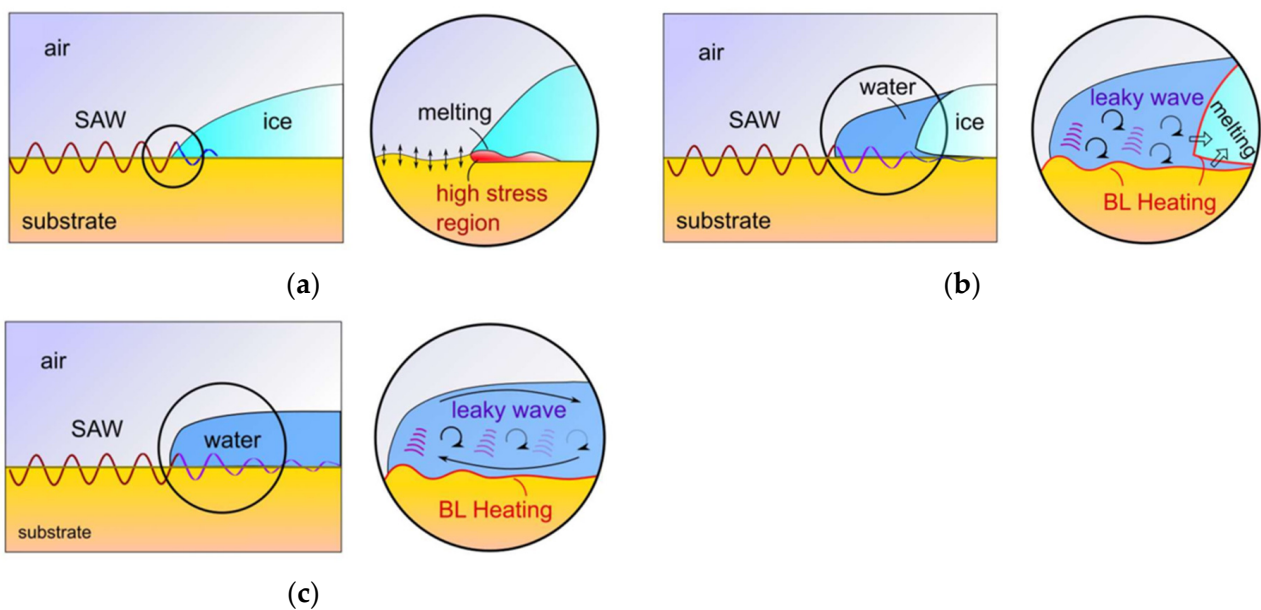


**Figure 12.** Sketch of the SAW-induced melting process of glaze ice aggregates: (a) initial deicing process: the SAW interacts with the ice, creating regions of high stresses. A thin water film forms in the high-stress region; (b) melting process: the SAW efficiently leaks into the water-film. The ice melts at the well-defined interface with the water; (c) active anti-icing process: the ice is completely melted. (BL: Boundary layer) [146].

Zeng et al. [147] experimentally demonstrated that SAWs can reduce ice adhesion. Nampoothiri et al. [148] deiced microliter-sized droplets with low-power SAW actuation using interdigitated electrodes on a piezoelectric ( $\text{LiNbO}_3$ ) substrate, suggesting the future development of efficient SAW-based deicing systems. Jacob et al. [146] demonstrated that energy-efficient deicing and prevention of ice formation could be achieved for larger volume piezoelectric substrates using high-frequency thickness-shear acoustic vibrations, with reduced ice adhesion. Jacob also attempted to transfer the deicing capability to low-thermal conductivity base materials.

### 5.6. Plasma Anti-Icing/Deicing

With the increasing research on active plasma flow control [149], attention has recently turned to the heating effect of the dielectric barrier discharge (DBD) actuator [150]. Especially, surface dielectric barrier discharge (SDBD) plasma has been found to be a

promising approach for efficient anti-icing due to its high heating performance, low energy consumption, quick response, and high efficiency [151].

Some studies have shown that plasma actuators are effective anti-icing/deicing devices, and nanosecond dielectric barrier discharge (NSDBD) plasma actuators have been found to perform better than alternating current DBD plasma actuators [152–155]. Zhu et al. [156,157] investigated the heating performance of NSDBD and demonstrated that it can heat up quickly and has an ice-proof heating effect. Wei et al. [158,159] showed that NSDBD had excellent anti-icing performance, removing an average ice thickness of 3 mm within 4 s and preventing further ice formation in the plasma protection zone.

Furthermore, Niu et al. [160] simulated the anti-icing effect of the NSDBD plasma actuator located at the NACA0012 wing leading edge. The simulation results demonstrated that the plasma actuator produced high-temperature air that covered the anti-icing area of NACA0012, preventing ice formation. Niu observed that higher peak voltage and pulse frequency of the plasma actuator led to better anti-icing performance, and directional arrangement optimization of the plasma excitation device could also improve its anti-icing capability. Thus, Niu concluded that the NSDBD plasma anti-icing technique was effective and could be used to develop anti-icing systems for unmanned aircraft.

Gao [161] developed a set of nanosecond pulse (ns-) SDBD plasma anti-icing devices for a certain type of all-weather small UAV. The working principle of ns-SDBD plasma actuators is as shown in Figure 13 [162]. The device has 8 kV voltage output, 200 A maximum output current, and 20 kHz heavy-frequency working capability and was designed with aircraft load, energy consumption, and anti-icing effectiveness as the top priorities. The experiment demonstrated that the device had anti-icing performance under specific icing conditions. The team plans to continue developing more compact, lighter, and durable anti-icing devices in the future.

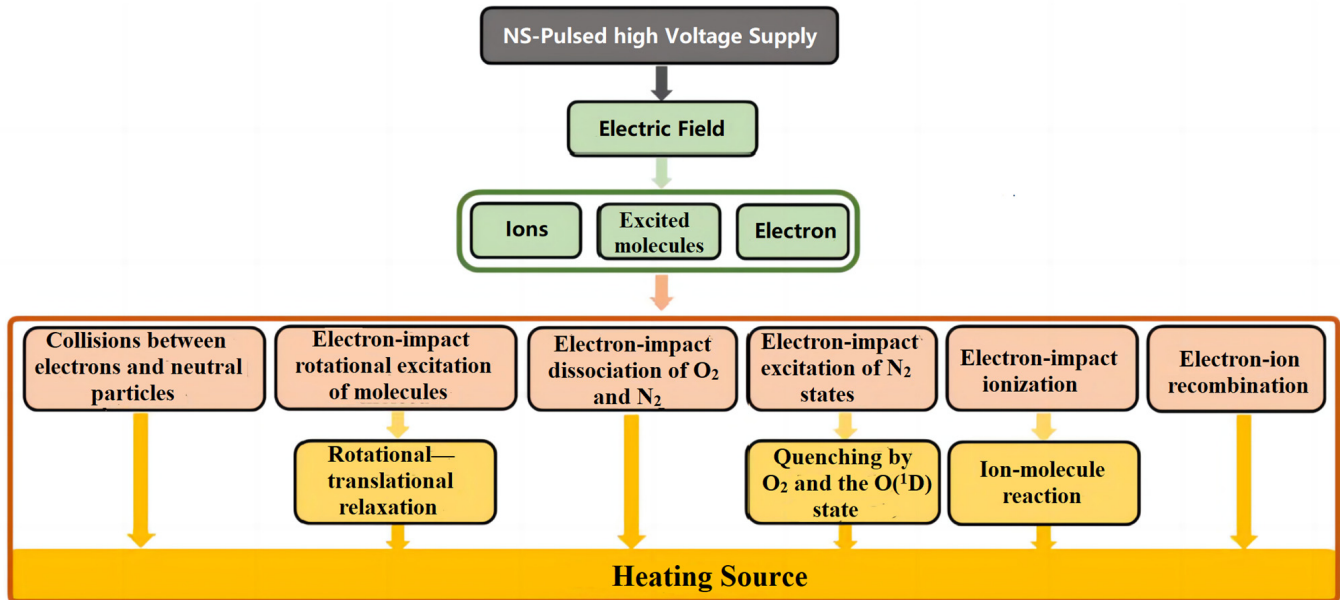


Figure 13. ns-SDBD plasma heating mechanism [162].

### 5.7. Synthetic Thermal Jet for Anti-Icing/Deicing

Since the mid-1990s, synthetic jet technology, also known as zero-mass-flux jet technology, has become a popular topic in flow control research. The technology synthesizes jets by combining controlled vortex structures. Synthetic jets are considered one of the most promising active flow control methods because of their advantages such as zero mass flow rate, low energy consumption, quick response, and flexible control [163]. The piezoelectric synthetic jet actuator (PSJA) was first proposed by Glezer, Smith, and their research team at Georgia Institute of Technology in the 1990s, attracting researchers from all over the world

due to its simple structure and high instantaneous pressure rise, making it potentially suitable as an ice breaker [164].

In 2013, Nikisha creatively proposed using a heated bottom synthetic jet actuator array to effectively control ice formation, studying the impact of parameters such as bottom heating, heating temperature, inflow temperature, droplet size, and distribution on ice formation [165–167]. Li designed a synthetic thermal jet actuator in 2015, based on a synthetic dual jet actuator [168,169]. The synthetic thermal actuator was to melt ice crystals on a cold surface in experiments on deicing principles, confirming the feasibility of deicing using synthetic thermal jets.

In 2017, Jiang [170] designed a novel electromagnetic synthetic dual jet actuator (as shown in Figure 14) for a specific UAV. By conducting fundamental experimental research on deicing an ice-covered wing using synthetic hot jets, it was found that the hot jet was more effective in reducing deicing time, by 25.0% up to 36.4%, when compared to pure heating deicing. Additionally, a 90° jet angle exhibited the most significant deicing effect, due to minimal momentum loss and enhanced heat transfer. Liu et al. added an impact rod structure to the traditional PSJA to improve its deicing performance in flight environments [171]. Furthermore, Gao et al. proposed a novel deicing strategy in which electric heating first eliminates the adhesion forces and then the PSJA discharge fractures the ice [172]. The PSJA operation only accounted for an insignificant 0.27% of the entire system's energy consumption and did not cause any surface bending.

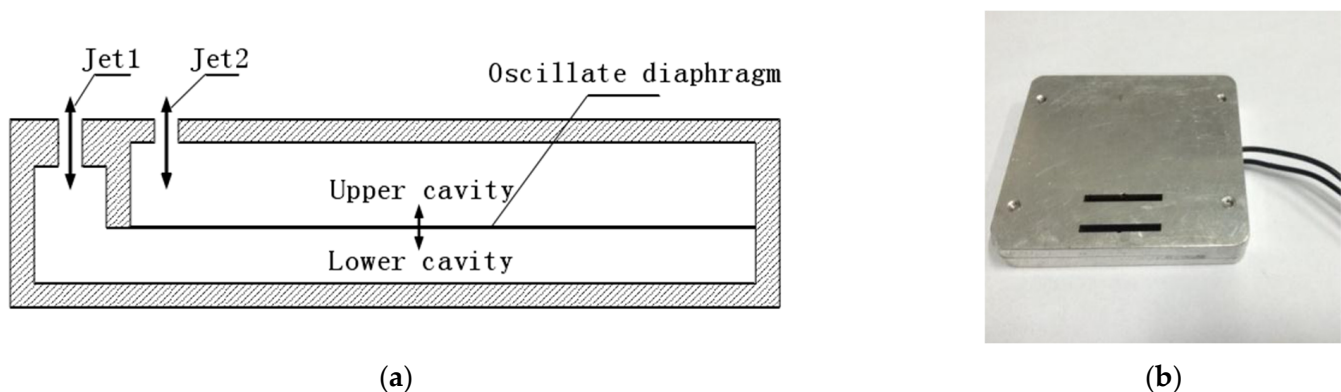


**Figure 14.** The synthetic double jet actuator's (a) structural schematic diagram and (b) physical diagram [170].

In general, the above-mentioned methods each have advantages and disadvantages. Airfoil and flight optimization as well as coatings are energy-efficient but only offer reductions or delays in icing. Electric heating systems have great anti-icing/deicing capabilities but consume more energy. Piezoelectric deicing can result in alterations to the surface shape of the aircraft. Plasma and synthetic thermal jet methods are not yet mature and lack practical applications. However, these methods are not mutually exclusive and can be combined. Under a framework of airfoil optimization, multiple anti-icing/deicing measures can be integrated, such as coatings with electric heating, synthetic thermal jet with electric heating, and piezoelectric with coatings. In conclusion, additional research and optimization are necessary to develop an outstanding anti-icing/deicing system for unmanned aircraft.

## 6. Discussions

Scholars have made advancements in studying the icing phenomenon and anti-icing/deicing techniques for UAVs, but there is still much progress to be made in effectively addressing icing challenges.

Currently, the academic community lacks a comprehensive understanding of the UAV icing phenomenon, particularly in relation to the complex flow behavior at low Reynolds

numbers, which remains unexplained accurately thus far. The most prominent methods for studying ice accretion are the icing wind tunnel experiment and numerical icing simulation. While existing icing numerical codes can reliably predict the accumulation of rime ice, they struggle to provide accurate forecasts for glaze and mixed ice due to the involvement of intricate physical factors. In addition, the icing wind tunnel tests on drones are not enough, and the mutual evidence between wind tunnel tests and numerical simulations is still insufficient. This lack of information not only makes it harder to understand icing on drones, but it also affects the assessment of anti-icing/deicing techniques. Considering the time-consuming and challenging nature of developing new icing numerical codes, as well as the existing codes' reliability, it is advisable to develop new models specifically for unmanned aircraft icing, apply them to the existing codes, and conduct extensive experiments to validate them.

On the contrary, the anti-icing/deicing system for UAVs must satisfy specific conditions such as low weight, minimal power consumption, and minimal aerodynamic design changes, due to constraints such as limited available energy, small size, light payload, and susceptibility to icing. However, some traditional anti-icing/deicing techniques cannot be used on drones, while others, although usable, cannot meet the above requirements. Therefore, developing an innovative approach becomes necessary when creating a novel anti-icing/deicing system for UAVs. Significantly improving the performance indicators of traditional techniques is not the only way. Developing new techniques is one approach, and considering the coupling of multiple ice mitigation techniques is also a good choice. In addition, the cost of anti-icing/deicing systems also needs to be considered.

## 7. Conclusions

The article provides a review of current knowledge regarding the icing phenomenon and anti-icing/deicing methods for fixed-wing UAVs. Previous studies show that UAV icing is similar to manned aircraft icing, but unique characteristics can arise due to the low Reynolds number, low flight speed, small size, low altitude, and different materials of most UAVs. In the limited research on UAV icing, it is still evident that icing poses severe hazards to UAVs. However, the existing anti-icing/deicing technology cannot meet the need of drones. The article discusses ice mitigation technology being explored and emphasizes the need for lightweight and energy-saving systems to reduce icing impact and ensure all-weather UAV operation.

**Author Contributions:** Conceptualization, L.Z. and X.Y.; methodology, L.Z. and X.Y.; investigation, L.Z. and Q.L.; data curation, L.Z.; writing—original draft preparation, L.Z.; writing—review and editing, L.Z. and X.Y.; supervision, X.Y. All authors have read and agreed to the published version of the manuscript.

**Funding:** The work reported in this paper is supported by National Natural Science Foundation of China (No. 12132019) & National Science and Technology Major Project of China (Project J2019-III-0010-0054).

**Data Availability Statement:** The data presented in this study are available on request from the corresponding author.

**Conflicts of Interest:** The authors declare no conflict of interest.

## Appendix A

Appendix A provides a summary of the research section of the main text. It includes selected content and is not exhaustive. Table A1 presents research on the icing principles and characteristics of drones. Table A2 presents ice mitigation techniques directly relevant to drones in Section 5.

**Table A1.** A tabular summary for UAV icing research.

Researchers	Year	Research Method	Major Achievement or Key Findings
Bottyán et al. [15]	2013	Flight tests	A UAV ice accretion model was developed.
Williams et al. [16]	2017	Flight tests and lab tests	The ice shapes differed significantly from those on high Reynolds number airfoils.
Matiychyk et al. [17]	2017	Flight tests	The energy consumption of unmanned aerial vehicles increased after icing.
Siddique [19]	2021	Flight tests	
Han et al. [20]	2023	Flight tests	
Avery [18]	2019	Flight tests	The geometric shape of ice driven by the flight flow field appeared on the surface of the drone.
Avery and Jacob [21]	2022	Numerical simulation and lab tests	A cylindrical volume icing model called ALRIA was established and validated.
Oswald et al. [22]	2022	Numerical simulation	The Spalart Allmaras turbulence model was limited in its applicability to estimating aerodynamic losses caused by ice at low Reynolds numbers.
Hann et al. [24]	2019	Numerical simulation and lab tests	The influence of airspeed on frost, mixed ice, and glaze increased sequentially. The relative ice thickness and relative ice limit of smaller airfoils significantly increased.
Hann et al. [26]	2020	Numerical simulation and lab tests	Spalart Allmaras and Menter's k- $\omega$ SST model had limitations in simulating complex ice shapes and stall. More complex icing caused greater degradation of flight performance. As the Reynolds number increased, lift increased while drag decreased.
Li et al. [27]	2019	Lab tests	The surface water reflux on the wing surface using thermoplastic materials was more pronounced [25].
Hann [32]	2018	Numerical simulation	LEWICE and FENSAP-ICE showed good consistency in simulating frost ice, while glaze and mixed ice showed significant differences.
Yirtici et al. [33]	2020	Numerical simulation	The resistance coefficient predicted by XFOIL method was in good agreement with experimental data, while the lift coefficient was not.
Muhammed and Virk [35]	2023	Numerical simulation	Transition k- $\omega$ SST turbulence model could accurately predict LSB, but it predicted an earlier separation start time.
Szilder and McIlwain [36]	2011	Numerical simulation	A UAV ice accretion model was developed. As the Reynolds number increased, ice changed from frost ice to mixed ice, and finally became clear ice.
Fajt et al. [39]	2019	Numerical simulation	Rising temperature caused an increase in ice mass. Ice caused an increase in resistance.
Cistriani et al. [43]	2007	Lab tests	Ice caused a decrease in lift.
Hann et al. [44]	2017	Numerical simulation	Ice accumulation increased drag while reducing lift and maximum angle of attack.
Szilder et al. [46]	2015	Numerical simulation	
Oo et al. [49]	2020	Lab tests	At low Reynolds numbers, flow reattachment delayed and separation increased.

**Table A2.** A tabular summary for ice mitigation techniques of UAVs.

Subject	Researchers	Year	Research Method	Major Achievement or Key Findings
Airfoil optimization	Li et al. [40]	2022	RADE algorithm	“PCE” airfoil had improved icing performance, with a 6.7% increase in maximum lift coefficient.
Flight optimization	Narum et al. [86]	2020	Particle swarm optimization	A 43% energy efficiency improvement or a 42% flight time reduction between two points.
Coatings	Ye et al. [97]	2021	Lab tests	A hydrophobic coating system that exhibited a contact angle $\theta \geq 115^\circ$ was created.
	Luo et al. [98]	2021	Lab tests	The PEEK-PEEK/PTFE/k-SiO <sub>2</sub> composite coatings for drone metal surfaces were created.
Electric heating combining with coatings	Hann et al. [117]	2021	Lab tests	The better design for layout of D•ICE was found.
	Roy et al. [119]	2021	Numerical simulation and lab tests	An integrated electrothermal anti-icing system using a thin etched foil heating film was designed and developed.
	Sørensen et al. [120]	2015	Numerical simulation and lab tests	A temperature-controlled anti-icing/deicing system for the airfoil of the X8 Skywalker UAV was designed.
	Yan et al. [127]	2023	Lab tests and flight tests	An anti-icing Skin with Micro-nano Structure was designed and tested.
Plasma	Zhu [128]	2018	Lab tests	A low-energy SHP electric heating anti-icing skin was created.
	Gao [164]	2021	Lab tests	A set of ns-SDBD plasma anti-icing device was created.
Synthetic thermal jet	Jiang [172]	2017	Lab tests	A novel electromagnetic synthetic dual jet actuator was designed.

## References

1. Weatherington, D.; Deputy, U. *Unmanned Aircraft Systems Roadmap, 2005–2030*; U.S. Department of Defense: Washington, DC, USA, 2005.
2. Gao, H.; Yu, P. The Application Prospects of Drones in Emergency Communication. *Labor. Prot.* **2022**, *85–87*. (In Chinese)
3. Villeneuve, E.; Karmouch, E.; Boulerice, X. Development of a small and transportable de-icing/anti-icing drone-mounted system. Part 1: System design. *Drone Syst. Appl.* **2022**, *10*, 155–177. [CrossRef]
4. Bragg, M.B.; Broeren, A.P.; Blumenthal, L.A. Iced-airfoil aerodynamics. *Prog. Aerosp. Sci.* **2005**, *41*, 323–362. [CrossRef]
5. How Is an UAV Affected by In-Flight Icing and Can We Simulate It Accurately? Available online: <https://uavicinglab.com/2021/05/28/how-is-an-uav-affected-by-in-flight-icing-and-can-we-simulate-it-accurately/> (accessed on 15 January 2022).
6. Haulman, D.L. *US Unmanned Aerial Vehicles in Combat 1991–2003*; Air Force Historical Research Agency: Montgomery, AL, USA, 2003.
7. Botura, G.; Fahrner, A. *Icing Detection System—Conception, Development, Testing and Applicability to UAVs*; AIAA-2003-6637; Goodrich Corp: Akron, OH, USA, 2003.
8. Szilder, K.; McIlwain, S. In-flight icing of UAVs—The influence of flight speed coupled with chord size. *Can. Aeronaut. Sp. J.* **2012**, *58*, 83–94. [CrossRef]
9. Zhang, B.; Tang, L.; Roemer, M. Probabilistic weather forecasting analysis for unmanned aerial vehicle path planning. *J. Guid. Control. Dyn.* **2014**, *37*, 309–312. [CrossRef]
10. Koenig, G.; Ryerson, C.; Larsson, J.; Reehorst, A. Effect of Variable LWC on Ice Shape in the NASA-GRC IRT. In Proceedings of the 41st Aerospace Sciences Meeting and Exhibit, Reno, NV, USA, 6–9 January 2003.

11. Lynch, F.; Khodadoust, A. Erratum to “Effects of ice accretions on aircraft aerodynamics”. *Prog. Aerosp. Sci.* **2002**, *38*, 669–767. [[CrossRef](#)]
12. Siquig, R.A. *Impact of Icing on Unmanned Aerial Vehicle (Uav) Operations*; Naval Environmental Protection Research Facility: Monterey, CA, USA, 1990.
13. Papadopoulos, C.; Ioannidou, S.; Panagiotou, P.; Yakinthos, K. Numerical investigation of the impact of tubercles and wing fences on the aerodynamic behaviour of a fixed-wing, tactical Blended-Wing-Body UAV platform. *IOP Conf. Ser. Mater. Sci. Eng.* **2022**, *1226*, 012015. [[CrossRef](#)]
14. Samad, A.; Villeneuve, E.; Blackburn, C.; Morency, F.; Volat, C. An Experimental Investigation of the Convective Heat Transfer on a Small Helicopter Rotor with Anti-Icing and De-Icing Test Setups. *Aerospace* **2021**, *8*, 96. [[CrossRef](#)]
15. Bottyán, Z. In-flight icing characteristics of unmanned aerial vehicles during special atmospheric condition over the carpathian-basin. *Landsc. Environ.* **2013**, *7*, 74–80.
16. Williams, N.B.A.; Brian, G.; Ol, M. The Effect of Icing on Small Unmanned Aircraft Low Reynolds Number Airfoils. In Proceedings of the 17th Australian International Aerospace Congress (AIAC), Melbourne, Australia, 26–28 February 2017.
17. Matiychyk, L.; Suvorova, N.; Tereshchenko, D.; Plakhotniuk, I.; Trachuk, K.; Komarova, K. Influence of Icing on Aircraft Performance of Unmanned Aerial Vehicle M-10-2 “Oko”. *Proc. Natl. Aviat. Univ.* **2017**, *4*, 52–59. [[CrossRef](#)]
18. Avery, A.S. Ice Accretion on Small Unmanned Aircraft. Ph.D. Thesis, Oklahoma State University, Stillwater, OK, USA, 2019.
19. Siddique, M.A. An Experimental Study on the Effects of Adverse Weathers on the Flight Performance of an Unmanned-Aerial-System (UAS). Ph.D. Thesis, Iowa State University, Ames, IA, USA, 2021.
20. Han, N.H.; Siddique, M.A.; Zhang, Z.C.; Tian, L.C.; Hu, H.Y.; Hu, H. A flight-testing campaign to examine inflight icing characteristics and its effects on the flight performance of an Unmanned-Aerial-Vehicle. *Cold Reg. Sci. Technol.* **2023**, *207*, 103775. [[CrossRef](#)]
21. Avery, A.S.; Jacob, J.D. Ice accretion panel model for cylinders at low Reynolds numbers. *Bull. Atmos. Sci. Technol.* **2022**, *3*, 7. [[CrossRef](#)]
22. Oswald, J.W.; Enache, A.; Hann, R.; Glabeke, G.; Lutz, T. UAV Icing: Experimental and Numerical Study of Glaze Ice Performance Penalties on an RG-15 Airfoil. In Proceedings of the AIAA SCITECH 2022 Forum, San Diego, CA, USA & Virtual, 3–7 January 2022.
23. Hann, R. UAV Icing: Ice Accretion Experiments and Validation. In Proceedings of the International Conference on Icing of Aircraft, Engines, and Structures, Minneapolis, MN, USA, 17–21 June 2019.
24. Hann, R.; Johansen, T.A. UAV icing: The influence of airspeed and chord length on performance degradation. *Aircr. Eng. Aerosp. Technol.* **2021**, *93*, 832–841. [[CrossRef](#)]
25. Hann, R. Atmospheric Ice Accretions, Aerodynamic Icing Penalties, and Ice Protection Systems on Unmanned Aerial Vehicles. Ph.D. Thesis, Norwegian University of Science and Technology, Trondheim, Norway, 2020.
26. Hann, R.; Hearst, R.J.; Sætran, L.; Bracchi, T. Experimental and Numerical Icing Penalties of an S826 Airfoil at Low Reynolds Numbers. *Aerospace* **2020**, *7*, 46. [[CrossRef](#)]
27. Li, L.K.; Liu, Y.; Zhang, Z.C.; Hu, H. Effects of thermal conductivity of airframe substrate on the dynamic ice accretion process pertinent to UAS inflight icing phenomena. *Int. J. Heat Mass Transf.* **2019**, *131*, 1184–1195. [[CrossRef](#)]
28. Anderson, D.N. Rime-, Mixed-, and Glaze-Iced Evaluations of Three Scaling Laws. In Proceedings of the 36th Aerospace Sciences Meeting and Exhibit, Reno, NV, USA, 10–13 January 1994.
29. Wright, W.B.; Bidwell, C.S. Additional improvements to the NASA Lewis ice accretion code LEWICE. In Proceedings of the 33rd Aerospace Sciences Meeting and Exhibit, Reno, NV, USA, 9–12 January 1995.
30. Beaugendre, H.; Morency, F.; Habashi, W.G. FENSAPICE: Roughness effects on ice shape prediction. *J. Aircr.* **2003**, *40*, 239–247. [[CrossRef](#)]
31. Hann, R.; Johansen, T.A. *Unsettled Topics in Unmanned Aerial Vehicle Icing*; SAE EDGE Research Report EPR2020008; SAE International: Warrendale, PA, USA, 2020.
32. Hann, R. UAV Icing: Comparison of LEWICE and FENSAP-ICE for Ice Accretion and Performance Degradation. In Proceedings of the 2018 Atmospheric and Space Environments Conference, Atlanta, GA, USA, 25–29 June 2018.
33. Yirtici, O.; Körpe, D.S.; Ozgen, S. Aerodynamic Performance Losses due to Ice Formation on the UAV’s Wing Profile. *J. Aeronaut. Space Technol.* **2020**, *13*, 207–215.
34. XFOIL Subsonic Airfoil Development System. Available online: <http://web.mit.edu/drela/Public/web/xfoil/> (accessed on 11 November 2019).
35. Muhammed, M.; Virk, M. Steady and Time Dependent Study of Laminar Separation Bubble (LSB) behavior along UAV Airfoil RG-15. *Int. J. Multiphysics* **2023**, *17*, 55–76.
36. Szilder, K.; McIlwain, S. *In-Flight Icing of UAVs—The Influence of Reynolds Number on the Ice Accretion Process*; SAE Technical Paper 2011-01-2572; SAE International: Warrendale, PA, USA, 2011.
37. Langmuir, I. *A Mathematical Investigation of Water Droplet Trajectories*; Army Air Forces Headquarters, Air Technical Service Command: San Antonio, TX, USA, 1946.
38. Koenig, G.; Ryerson, C.; Kmiec, R. UAV Icing Flight Simulation. In Proceedings of the 40th AIAA Aerospace Sciences Meeting & Exhibit, Reno, NV, USA, 14–17 January 2002.
39. Fajt, N.; Hann, R.; Lutz, T. The Influence of Meteorological Conditions on the Icing Performance Penalties on a UAV Airfoil. In Proceedings of the 8th European Conference for Aeronautics and Space Sciences (EUCASS), Madrid, Spain, 1–4 July 2019.

40. Li, H.; Zhang, Y.; Chen, H. Optimization design of airfoils under atmospheric icing conditions for UAV. *Chin. J. Aeronaut.* **2022**, *35*, 118–133. [[CrossRef](#)]
41. Bottyán, Z. Estimation of In-Flight Icing Characteristics of UAVs during Different Meteorological Conditions. In Proceedings of the 8th International Conference on Intelligent Unmanned Systems (ICIUS 2012), Singapore, 22 October 2012.
42. Jeck, R.K. *A History and Interpretation of Aircraft Icing Intensity Definitions and FAA Rules for Operating in Icing Conditions*; Federal Aviation Administration Technical Report DOT/FAA/AR-01/91; SKYbrary: Anklam, Germany, 2001.
43. Cistriani, L. Falco UAV Low Reynolds Airfoil Design and Testing at Galileo Avionica. In *UAV Design Processes/Design Criteria for Structures*; Galileo Avionica Ronchi Dei Legionari (Italy) Simulators and Uav Business Unit; RTO: Neuilly-sur-Seine, France, 2007.
44. Hann, R.; Wenz, A.; Gryte, K.; Johansen, T.A. Impact of Atmospheric Icing on UAV Aerodynamic Performance. In Proceedings of the 2017 Workshop on Research, Education and Development of Unmanned Aerial Systems (RED-UAS), Linköping, Sweden, 3–5 October 2017.
45. Oswald, J.W. UAV Icing: Numerical and Experimental Study of Performance Penalties on an RG-15 Airfoil. Master's Thesis, University of Stuttgart, Stuttgart, Germany, 2021.
46. Szilder, K.; Yuan, W. The Influence of Ice Accretion on the Aerodynamic Performance of a UAS Airfoil. In Proceedings of the 53rd AIAA Aerospace Sciences Meeting, Kissimmee, FL, USA, 5–9 January 2015.
47. Hain, R.; Kähler, C.; Radespiel, R. Dynamics of laminar separation bubbles at low-Reynolds-number airfoils. *J. Fluid Mech.* **2009**, *630*, 129–153. [[CrossRef](#)]
48. O'Meara, M.M.; Mueller, T.J. Laminar Separation Bubble Characteristics on an Airfoil at Low Reynolds Numbers. *AIAA J.* **1987**, *25*, 1033–1041. [[CrossRef](#)]
49. Oo, N.L.; Richards, P.J.; Sharma, R.N. Ice-Induced Separation Bubble on RG-15 Airfoil at Low Reynolds Number. *AIAA J.* **2020**, *58*, 5156–5167. [[CrossRef](#)]
50. Ericsson, L.E.; Reding, J.P. *Unsteady Airfoil Stall*; NASA Report CR-66787; NASA Center for Aerospace Information: Hanover, MD, USA, 1969.
51. Lissaman, P.B.S. Low-Reynolds-number airfoils. *Annu. Rev. Fluid Mech.* **1983**, *15*, 223–239. [[CrossRef](#)]
52. Seifert, H.; Richert, F. Aerodynamics of Iced Airfoils and Their Influence on Loads and Power Production. In Proceedings of the European Wind Energy Conference, Dublin, Ireland, 6–9 October 1997; pp. 459–460.
53. Jasinski, W.J.; Selig, M.S.; Bragg, M.B.; Shawn, C.N. Wind Turbine Performance Under Icing Conditions. *J. Sol. Energy Eng.* **1998**, *120*, 60–65. [[CrossRef](#)]
54. Oo, N.L.; Richards, P.; Sharma, R. Influence of an Ice-Induced Separation Bubble on the Laminar Separation Bubble on an RG-15 Airfoil at Low Reynolds Numbers. In Proceedings of the AIAA Aviation 2020 Forum, Virtual, 15–19 June 2020.
55. Muhammed, M.; Virk, M.S. Ice Accretion on Fixed-Wing Unmanned Aerial Vehicle—A Review Study. *Drones* **2022**, *6*, 86. [[CrossRef](#)]
56. Wang, J.; Ji, S.Y.; Yi, X.S.; Zhao, W.M. Research progress in aircraft anti-icing/deicing technology. *Aviat. Manuf. Technol.* **2015**, *495*, 30–32. (In Chinese)
57. Cornell, J.S.; Pillard, D.A.; Hernandez, M.T. Comparative measures of the toxicity of component chemicals in aircraft deicing fluid. *Environ. Toxicol. Chem.* **2000**, *19*, 1465–1472. [[CrossRef](#)]
58. Sapienza, R. Environmentally Benign Anti-Icing or Deicing Fluids. U.S. Patent 6,129,857, 2000.
59. *Unmanned Aerial Vehicle Reliability Study*; Technical Report; Office of the Secretary of Defense: Washington, DC, USA, 2003.
60. Peck, L.; Ryerson, C.; Martel, C. *Army Aircraft Icing*; Technical Report; Cold Regions Research and Engineering Laboratory: Hanover, HA, USA, 2002.
61. GA-ASI's MQ-9B RPAS Undergoes Cold Weather Validation Test. Available online: <https://www.airforce-technology.com/news/gaasis-mq9b-cold-weather-validation> (accessed on 27 February 2022).
62. Dong, W.; Zhu, J.; Zheng, M.; Chen, Y. Thermal analysis and testing of nonrotating cone with hot-air anti-icing system. *J. Propuls. Power* **2015**, *31*, 3. [[CrossRef](#)]
63. Boinovich, L.B.; Emelyanenko, A.M. Anti-icing Potential of Superhydrophobic Coatings. *Mendeleev Commun* **2013**, *23*, 3–10. [[CrossRef](#)]
64. Farzaneh, M.; Ryerson, C.C. Anti-icing and deicing techniques. *Cold Reg. Sci. Technol.* **2011**, *65*, 88–96. [[CrossRef](#)]
65. Shen, Y.Z.; Wu, Y.; Tao, J.; Zhu, C.L.; Chen, H.F.; Wu, Z.W.; Xie, Y.H. Spraying Fabrication of Durable and Transparent Coatings for Anti-Icing Application: Dynamic Water Repellency, Icing Delay, and Ice Adhesion. *ACS Appl. Mater. Interfaces* **2019**, *11*, 3590–3598. [[CrossRef](#)] [[PubMed](#)]
66. Lv, J.Y.; Song, Y.L.; Jiang, L.; Wang, J.J. Bio-Inspired Strategies for Anti-Icing. *ACS Nano* **2014**, *8*, 3152–3169. [[CrossRef](#)] [[PubMed](#)]
67. Varanasi, K.K.; Hsu, M.; Bhate, N.; Yang, W.S.; Deng, T. Spatial control in the heterogeneous nucleation of water. *Appl. Phys. Lett.* **2009**, *95*, 094101. [[CrossRef](#)]
68. Strobl, T.; Storm, S.; Thompson, D.; Hornung, M.; Thielecke, F. Feasibility study of a hybrid ice protection system. *J. Aircr.* **2015**, *52*, 2064–2076. [[CrossRef](#)]
69. Fortin, G.; Adomou, M.; Perron, J. *Experimental Study of Hybrid Anti-Icing Systems Combining Thermoelectric and Hydrophobic Coatings*; SAE Technical Paper 2011-38-0003; SAE International: Warrendale, PA, USA, 2011.
70. Ma, L.; Xiong, L.; Liu, L.; Yang, J. Experimental study on electro-thermal deicing technique for carbon fiber composite. *Acta Aeronaut. Astronaut. Sin.* **2012**, *33*, 54–61. (In Chinese)

71. Jiang, H.; Wang, H.T.; Liu, G.; Liu, J.P.; Zhang, X.N.; Chen, Y.Q.; Zhou, W.W. Light-weight, flexible, low-voltage electro-thermal film using graphite nanoplatelets for wearable/smart electronics and deicing devices. *J. Alloys Compd.* **2017**, *699*, 1049–1056. [[CrossRef](#)]
72. Rutherford, R.B. De-Ice and Anti-Ice System and Method for Aircraft Surfaces. U.S. Patent 6194685B1, 27 February 2001.
73. Buschhorn, S.T.; Kessler, S.S.; Lachmann, N.; Gavin, J.; Thomas, G.; Wardle, B.L. Electrothermal Icing Protection of Aerosurfaces Using Conductive Polymer Nanocomposites. In Proceedings of the 54th AIAA/ASME/ASCE/AHS/ASC Structures, Structural Dynamics, and Materials Conference, Boston, MA, USA, 8–11 April 2013; p. 1729.
74. Strehlow, R.H.; Moser, R. *Capitalizing on the Increased Flexibility that Comes from High Power Density Electrothermal Deicing*; SAE Technical Paper, 2009-01-3165; SAE International: Warrendale, PA, USA, 2009.
75. China's Domestically Produced Large-Scale Unmanned Aerial Vehicle Used for Artificial Weather Modification, the Wing Loong II, Successfully Completed Its Maiden Flight and Got First Place. Available online: <http://www.iliema.cn/article-661981-1.html> (accessed on 9 January 2022). (In Chinese).
76. Guang-Chao, L.I.; Jiang, H.E.; Lin, G.P. Electro-impulse de-icing (EIDI) technology study. *J. Aerosp. Power* **2011**, *26*, 1728–1735.
77. Zumwalt, G.; Friedberg, R. Designing an Electro-Impulse De-Icing System. In Proceedings of the 24th Aerospace Sciences Meeting, Reno, NV, USA, 6–9 January 1986.
78. Orion UAV Can Perform Ice Reconnaissance in the Arctic. Available online: <https://www.airrecognition.com/index.php/news/defense-aviation-news/2021/october/7733-orion-uav-can-perform-ice-reconnaissance-in-the-arctic.html> (accessed on 11 October 2021).
79. Ghisu, T.; Jarrett, J.P.; Parks, G.T. Robust design optimization of airfoils with respect to ice accretion. *J. Aircr.* **2011**, *48*, 287–304. [[CrossRef](#)]
80. Li, H.; Zhang, Y.; Chen, H. Optimization of supercritical airfoil considering the ice-accretion effects. *AIAA J.* **2019**, *57*, 4650–4669. [[CrossRef](#)]
81. Dai, J.Z.; Li, H.R.; Zhang, Y.F.; Chen, H.X. Optimization of multi-element airfoil settings considering ice accretion effect. *Chin. J. Aeronaut.* **2023**, *36*, 41–57. [[CrossRef](#)]
82. Vukits, T.J. Overview and Risk Assessment of Icing for Transport Category Aircraft And Components. In Proceedings of the 40th AIAA Aerospace Sciences Meeting and Exhibit, Reno, NV, USA, 14–17 January 2002.
83. Thompson, G. High Resolution Numerical Weather Model Forecasts of Icing at the Ground and in the Air. In Proceedings of the International Workshop on Atmospheric Icing of Structures, Reykjavík, Iceland, 23–28 June 2019.
84. Niu, J.; Sang, W.; Li, D.; Guo, Q.; Qiu, A.; Shi, M. Fast Prediction of Multiple Parameters Related to Iced Airfoil Based on POD and Kriging Methods. *J. Appl. Fluid Mech.* **2023**, *16*, 325–336. [[CrossRef](#)]
85. Hovenburg, A.; de Alcantara Andrade, F.A.; Hann, R.; Dahlin Rodin, C.; Johansen, T.; Storvold, R. Long range path planning using an aircraft performance model for battery powered sUAS equipped with icing protection system. *IEEE J. Miniaturization Air Space Syst.* **2020**, *1*, 76–89. [[CrossRef](#)]
86. Narum, E.F.L.; Hann, R.; Johansen, T.A. Optimal Mission Planning for Fixed-Wing UAVs with Electro-Thermal Icing Protection and Hybrid-Electric Power System. In Proceedings of the 2020 International Conference on Unmanned Aircraft Systems (ICUAS), Athens, Greece, 1–4 September 2020; pp. 651–660.
87. Subramanyam, B.S.; Kondrashov, V.; Ruhe, J.; Varanasi, K.K. Low ice adhesion on nano-textured superhydrophobic surfaces under supersaturated conditions. *ACS Appl. Mater. Interfaces* **2016**, *8*, 12583–12587. [[CrossRef](#)] [[PubMed](#)]
88. Guo, P.; Zheng, Y.; Wen, M.; Song, C.; Lin, Y.; Jiang, L. Icephobic/anti-icing properties of micro/nanostructured surfaces. *Adv. Mater.* **2012**, *24*, 2642–2648. [[CrossRef](#)] [[PubMed](#)]
89. Kim, P.; Wong, T.-S.; Alvarenga, J.; Kreder, M.J.; Adorno-Martinez, W.E.; Aizenberg, J. Liquid-infused nanostructured surfaces with extreme anti-ice and anti-frost performance. *ACS Nano* **2012**, *6*, 6569–6577. [[CrossRef](#)]
90. Liu, Q.; Yang, Y.; Huang, M.; Zhou, Y.; Liu, Y.; Liang, X. Durability of a lubricant-infused electro-spray silicon rubber surface as an anti-icing coating. *Appl. Surf. Sci.* **2015**, *346*, 68–76. [[CrossRef](#)]
91. Ozbay, S.; Yuceel, C.; Erbil, H.Y. Improved icephobic properties on surfaces with a hydrophilic lubricating liquid. *ACS Appl. Mater. Interfaces* **2015**, *7*, 22067–22077. [[CrossRef](#)]
92. Chen, J.; Luo, Z.; Fan, Q.; Lv, J.; Wang, J. Anti-ice coating inspired by ice skating. *Small* **2014**, *10*, 4693–4699. [[CrossRef](#)]
93. Dou, R.; Chen, J.; Zhang, Y.; Wang, X.; Cui, D.; Song, Y.; Jiang, L.; Wang, J. Anti-icing coating with an aqueous lubricating layer. *ACS Appl. Mater. Interfaces* **2014**, *6*, 6998–7003. [[CrossRef](#)]
94. Zhao, Z.; Chen, H.; Liu, X.; Liu, H.; Zhang, D. Development of high-efficient synthetic electric heating coating for anti-icing/de-icing. *Surf. Coat. Technol.* **2018**, *349*, 340–346. [[CrossRef](#)]
95. Matsubayashi, T.; Tenjimbayashi, M.; Manabe, K.; Komine, M.; Navarrini, W.; Shiratori, S. Integrated anti-icing property of super-repellency and electrothermogenesis exhibited by PEDOT:PSS/cyanoacrylate composite nanoparticles. *ACS Appl. Mater. Interfaces* **2016**, *8*, 24212–24220. [[CrossRef](#)] [[PubMed](#)]
96. Ye, W.M.; Guo, K.; Qiu, W.P. Research and development of anti icing and hydrophobic coatings for unmanned aerial vehicles. *Mech. Electr. Inf.* **2021**, *672*, 18–20. (In Chinese)
97. Luo, H.Y.; Li, Y.; Huan, D.J.; Zhu, C.L.; Wang, J.X.; Zeng, D. Efficient Fabrication of Wear-Resistant PEEK Matrix Composite Coating with Superhydrophobicity for Self-Cleaning and Anti-Icing Applications. *Polym.-Plast. Technol. Mater.* **2021**, *60*, 1106–1121. [[CrossRef](#)]

98. Wong, T.S.; Kang, S.H.; Tang, S.K.Y.; Smythe, E.J.; Hatton, B.D.; Grinthal, A.; Aizenberg, J. Bioinspired self-repairing slippery surfaces with pressure-stable omniphobicity. *Nature* **2011**, *477*, 443–447. [CrossRef] [PubMed]
99. Liu, X.L.; Chen, H.W.; Zhao, Z.H.; Yan, Y.Y.; Zhang, D.Y. Slippery liquid-infused porous electric heating coating for anti-icing and deicing applications. *Surf. Coat. Technol.* **2019**, *374*, 889–896. [CrossRef]
100. Hann, R.; Borup, K.; Zolich, A.; Sorensen, K.; Vestad, H.; Steinert, M.; Johansen, T. *Experimental Investigations of an Icing Protection System for UAVs*; SAE Technical Paper 2019-01-2038; SAE International: Warrendale, PA, USA, 2019.
101. Zhao, Z.H.; Chen, H.W.; Liu, X.L.; Wang, Z.L.L.; Zhu, Y.T.; Zhou, Y.P. The development of electric heating coating with temperature controlling capability for anti-icing/de-icing. *Cold Reg. Sci. Technol.* **2021**, *184*, 103234. [CrossRef]
102. Yao, X.D.; Hawkins, S.C.; Falzon, B.G. An advanced anti-icing/de-icing system utilizing highly aligned carbon nanotube webs. *Carbon* **2018**, *136*, 130–138. [CrossRef]
103. Pan, L.; Liu, Z.; Kiziltaş, O.; Zhong, L.; Pang, X.; Wang, F.; Zhu, Y.; Ma, W.; Lv, Y. Carbon fiber/poly ether ether ketone composites modified with graphene for electro-thermal deicing applications. *Compos. Sci. Technol.* **2020**, *192*, 108117. [CrossRef]
104. Karim, N.; Zhang, M.; Afroj, S.; Koncherry, V.; Potluri, P.; Novoselov, K.S. Graphene-based surface heater for de-icing Applications. *RSC Adv.* **2018**, *8*, 16815–16823. [CrossRef]
105. Cortés, A.; Romate, X.F.S.; Jiménez-Suárez, A.; Campo, M.; Prolongo, M.G.; Ureña, A.; Prolongo, S.G. 3D printed anti-icing and de-icing system based on CNT/GNP doped epoxy composites with self-curing and structural health monitoring capabilities. *Smart Mater. Struct.* **2021**, *30*, 025016. [CrossRef]
106. Wang, T.; Zheng, Y.; Raji, A.-R.O.; Li, Y.; Sikkwma, W.K.A.; Tour, J.M. Passive anti-icing and active deicing films. *ACS Appl Mater Interfaces* **2016**, *8*, 14169–14173. [CrossRef] [PubMed]
107. Falin, A.; Cai, Q.; Santos, E.J.G.; Scullion, D.; Qian, D.; Zhang, R.; Yang, Z.; Huang, S.; Watanabe, K.; Taniguchi, T.; et al. Mechanical properties of atomically thin boron nitride and the role of interlayer interactions. *Nat. Commun.* **2017**, *8*, 15815. [CrossRef] [PubMed]
108. Thomassin, J.-M.; Jérôme, C.; Pardoën, T.; Bailly, C.; Huynen, I.; Detrembleur, C. Polymer/carbon based composites as electromagnetic interference (EMI) shielding materials. *Mater. Sci. Eng. R Rep.* **2013**, *74*, 211–232. [CrossRef]
109. Hwang, H.; Ma, K.Y.; Kim, J.W.; Yuk, D.; Hong, J.; Jung, J.H.; Yong, S.; Choi, J.; Kim, J.Y.; Shin, H.S. Radio-frequency-transmitting hexagonal boron nitride-based antiand de-icing heating system. *Nanoscale* **2020**, *12*, 21895–21900. [CrossRef] [PubMed]
110. Vertuccio, L.; De Santis, F.; Pantani, R.; Lafdi, K.; Guadagno, L. Effective de-icing skin using graphene-based flexible heater. *Compos. Part B Eng.* **2019**, *162*, 600–610. [CrossRef]
111. Ming, Y.K.; Duan, Y.G.; Zhang, S.Q.; Zhu, Y.; Wang, B.W. Self-heating 3D printed continuous carbon fiber/epoxy mesh and its application in wind turbine deicing. *Polym. Test.* **2020**, *82*, 106309. [CrossRef]
112. Galao, O.; Bañón, L.; Baeza, F.; Carmona, J.; Garcés, P. Highly conductive carbon fiber reinforced concrete for icing prevention and curing. *Materials* **2016**, *9*, 281. [CrossRef]
113. Zhao, H.; Wu, Z.; Wang, S.; Zheng, J.; Che, G. Concrete pavement deicing with carbon fiber heating wires *Cold Reg. Sci. Technol.* **2011**, *65*, 413–420.
114. Idris, M.K.; Qiu, J.F.; Melenka, G.W.; Grau, G. Printing electronics directly onto carbon fiber composites: Unmanned aerial vehicle (UAV) wings with integrated heater for de-icing. *Eng. Res. Express* **2020**, *2*, 025022. [CrossRef]
115. Xu, X.; Wang, F.; Mao, J. The flexible pressure-sensitive adhesive graphene-based composite heater based on the laminating structure for de-icing applications. *J. Mater. Sci. Mater. Electron.* **2021**, *32*, 13994–14005. [CrossRef]
116. Hann, R.; Enache, A.; Nielsen, M.C.; Stovner, B.N.; Beeck, J.V.; Johansen, T.A.; Borup, K.T. Experimental Heat Loads for Electrothermal Anti-Icing and De-Icing on UAVs. *Aerospace* **2021**, *8*, 83. [CrossRef]
117. SAE International. *Ice, Rain, Fog, and Frost Protection*; Aerospace Information Report AIR1168/4; SAE International: Warrendale, PA, USA, 2016.
118. Roy, R.; Raj, L.P.; Jo, J.-H.; Cho, M.-Y.; Kweon, J.-H.; Myong, R.S. Multiphysics anti-icing simulation of a CFRP composite wing structure embedded with thin etched-foil electrothermal heating films in glaze ice conditions. *Compos. Struct.* **2021**, *276*, 114441. [CrossRef]
119. Sørensen, K.L.; Helland, A.S.; Johansen, T.A. Carbon Nanomaterial-Based Wing Temperature Control System for In-Flight Anti-Icing and De-Icing of Unmanned Aerial Vehicles. In Proceedings of the IEEE Aerospace Conference Proceedings, Big Sky, MT, USA, 7–14 March 2015.
120. Sørensen, K.L.; Johansen, T.A. Thermodynamics of a Carbon Nano-Materials Based Icing Protection System for Unmanned Aerial Vehicle. In Proceedings of the IEEE Aerospace Conference, Big Sky, MT, USA, 5–12 March 2016.
121. Warwick, G. Nanotech promises energy-efficient anti-icing. *Aviat. Week Space Technol.* **2012**, *174*, 15.
122. Grinats, É.S.; Miller, A.B.; Potapov, Y.F.; Stasenko, A.L. Experimental and theoretical investigations of the processes of icing of nanomodified superhydrophobic and ordinary surfaces. *Vestn. Moskovsk. Gos. Obl. Univ. Ser. Fiz.-Mat.* **2013**, *3*, 84–92.
123. Bogoslov, E.A.; Danilaev, M.P.; Mikhailov, S.A.; Pol'skii, Y.E. Energy efficiency of an integral anti-ice system based on fluoroplastic films. *J. Eng. Phys. Thermophys.* **2016**, *89*, 815–820. [CrossRef]
124. Battelle's Anti-Icing System for Remotely Piloted Aircraft (RPAs). Available online: <http://www.battelle.org> (accessed on 14 August 2013).
125. Yan, Z.X.; He, Y.; Yuan, W.Z.; Yuan, W.Z. Anti-icing Skin with Micro-nano Structure Inspired by *Fargesia Qinlingensis*. *Trans. Nanjing Univ. Aeronaut. Astronaut.* **2023**, *2*, 115–123.

126. Zhu, B. Low Power Superhydrophobic Electrothermal Skin and Its Anti-icing Performance. Master's Thesis, Northwestern Polytechnical University, Xi'an, China, 2018. (In Chinese).
127. Deshpande, S.; Sæterdal, A.; Sundsbø, P.-A. Sea Spray Icing: The physical process and review of prediction models and winterization techniques. *J. Offshore Mech. Arct. Eng.* **2021**, *143*, 061601. [[CrossRef](#)]
128. Villeneuve, E.; Harvey, D.; Zimcik, D.; Aubert, R.; Perron, J. Piezoelectric deicing system for rotorcraft. *J. Am. Helicopter Soc.* **2015**, *60*, 1–12. [[CrossRef](#)]
129. Venna, S.V.; Lin, Y.J. In-Flight De-Icing Self-Actuating Wing Structures with Piezoelectric Actuators. In Proceedings of the American Society of Mechanical Engineers/International Mechanical Engineering Congress and Exposition, New Orleans, LA, USA, 17–22 November 2002; pp. 237–245.
130. Yao, S.J. Research on Wing Deicing Method Based on Piezoelectric Drivers. Master's Thesis, Nanjing University of Aeronautics and Astronautics, Nanjing, China, 2010.
131. Bai, T. Ice Detection and Deicing Method Based on Piezoelectric Materials. Ph.D. Thesis, Nanjing University of Aeronautics and Astronautics, Nanjing, China, 2015.
132. Palacios, J.; Smith, E.; Rose, J.; Royer, R. Ultrasonic de-icing of wind-tunnel impact icing. *J. Aircr.* **2011**, *48*, 1020–1027. [[CrossRef](#)]
133. Palacios, J.; Smith, E.; Rose, J. Investigation of an Ultrasonic Ice Protection System for Helicopter Rotor Blades. *Annu. Forum Proc.—AHS Int.* **2008**, *1*, 609–618.
134. Tarquini, S.; Antonini, C.; Amirfazli, A.; Marengo, M.; Palacios, J. Investigation of Ice Shedding Properties of Superhydrophobic Coatings on Helicopter Blades. *Cold Reg. Sci. Technol.* **2014**, *100*, 50–58. [[CrossRef](#)]
135. Overmeyer, A.; Palacios, J.; Smith, E. Ultrasonic de-icing bondline design and rotor ice testing. *AIAA J.* **2013**, *51*, 2965–2976. [[CrossRef](#)]
136. Budinger, M.; Pommier-Budinger, V.; Napias, G.; Silva, A.C. Ultrasonic ice protection systems: Analytical and numerical models for architecture tradeoff. *J. Aircr.* **2016**, *53*, 680–690. [[CrossRef](#)]
137. Venna, S.V.; Lin, Y.J. Development of Self-Actuating In-Flight De-Icing Structures with Power Consumption Considerations. In Proceedings of the American Society of Mechanical Engineers International Mechanical Engineering Congress and Exposition, Washington, DC, USA, 17–22 November 2003; pp. 45–53.
138. Venna, S.V.; Lin, Y.J. Mechatronic Development of Self-Actuating In-Flight De-Icing Structures. *IEEE/ASME Trans. Mechatron.* **2006**, *11*, 585–592. [[CrossRef](#)]
139. Venna, S.; Lin, Y.J.; Botura, G. Piezoelectric Transducer Actuated Leading Edge De-Icing with Simultaneous Shear and Impulse Forces. *J. Aircr.* **2007**, *44*, 509–515. [[CrossRef](#)]
140. Struggl, S.; Korak, J.; Feyrer, C. A Basic Approach for Wing Leading De-Icing by Smart Structures. In Proceedings of the SPIE Smart Structures and Materials + Nondestructive Evaluation and Health Monitoring, San Diego, CA, USA, 6–10 March 2011.
141. Palanque, V. Design of Low Consumption Electro-Mechanical De-Icing Systems. Ph.D. Thesis, Université de Toulouse ISAE-Supaero, Toulouse, France, 2022.
142. Tan, M.K.; Friend, J.R.; Yeo, L.Y. Interfacial Jetting Phenomena Induced by Focused Surface Vibrations. *Phys. Rev. Lett.* **2009**, *103*, 024501. [[CrossRef](#)]
143. Qi, A.; Yeo, L.Y.; Friend, J.R. Interfacial Destabilization and Atomization Driven by Surface Acoustic Waves. *Phys. Fluids* **2008**, *20*, 074103. [[CrossRef](#)]
144. Li, L.; Wu, E.; Jia, K.; Yang, K. Temperature Field Regulation of a Droplet Using an Acoustothermal Heater. *Lap Chip* **2021**, *21*, 3184–3194. [[CrossRef](#)]
145. Mehmood, M.; Nawaz Chaudhary, T.; Burnside, S.; Khan, U.F.; Yongqing Fu, R.; Chen, B. Coupling Mechanism of Kinetic and Thermal Impacts of Rayleigh Surface Acoustic Waves on the Microdroplet. *Exp. Therm. Fluid Sci.* **2022**, *133*, 110580. [[CrossRef](#)]
146. Jacob, S.; Pandey, S.; Moral, J.D.; Karimzadeh, A.; Gil-Rostra, J.; González-Elipe, A.R.; Borrás, A.; Winkler, A. Surface Acoustic Waves Equip Materials with Active Deicing Functionality: Unraveled Deicing Mechanisms and Application to Centimeter Scale Transparent Surfaces. *Adv. Mater. Technol.* **2023**, *8*, 2300263. [[CrossRef](#)]
147. Zeng, X.; Yan, Z.; Lu, Y.; Fu, Y.; Lv, X.; Yuan, W.; He, Y. Reduction of Ice Adhesion Using Surface Acoustic Waves: Nanoscale Vibration and Interface Heating Effects. *Langmuir* **2021**, *37*, 11851–11858. [[CrossRef](#)] [[PubMed](#)]
148. Nampoothiri, K.N.; Nath, A.; Satpathi, N.S.; Sen, A.K. Deicing of Sessile Droplets Using Surface Acoustic Waves. *Langmuir* **2023**, *39*, 3934–3941. [[CrossRef](#)] [[PubMed](#)]
149. Roth, J.R.; Sherman, D.M.; Wilkinson, S.P. Boundary Layer Flow Control with a One Atmosphere Uniform Glow Discharge Surface Plasma. In Proceedings of the 36th AIAA Aerospace Sciences Meeting and Exhibit, Reno, NV, USA, 12–15 January 1998. AIAA-98-0328.
150. Winkel, R.; Correale, G.; Kotsonis, M. Effect of Dielectric Material on Thermal Effect Produced by ns-DBD Plasma Actuator. In Proceedings of the 45th AIAA Plasma Dynamics and Lasers Conference, Atlanta, GA, USA, 16–20 June 2014. AIAA-2014-2119.
151. Li, Q.Q.; Hao, L.Y. Surface Dielectric Barrier Discharge Plasma and Its Applications. *High Volt. Technol.* **2016**, *42*, 1079–1090. (In Chinese)
152. Cai, J.; Tian, Y.; Meng, X.; Han, X.; Zhang, D.; Hu, D. An experimental study of icing control using DBD plasma actuator. *Exp. Fluids* **2017**, *58*, 102. [[CrossRef](#)]

153. Kolbakir, C.; Liu, Y.; Starikovskiy, A.; Miles, R.B.; Hu, H. An Experimental Investigation on The Thermal Effects of NS-DBD and AC-DBD Plasma Actuators for Aircraft Icing Mitigation. In Proceedings of the AIAA Science and Technology Forum and Exposition, Kissimmee, FL, USA, 8–12 January 2018. AIAA-2018-0164.
154. Liu, Y.; Hu, H. An experimental investigation on the unsteady heat transfer process over an ice accreting airfoil surface. *Int. J. Heat Mass Transf.* **2018**, *122*, 707–718. [[CrossRef](#)]
155. Liu, Y.; Kolbakir, C.; Hu, H. A Comparison Study on AC-DBD Plasma and Electrical Heating for Aircraft Icing Mitigation. In Proceedings of the AIAA Science and Technology Forum and Exposition, Kissimmee, FL, USA, 8–12 January 2018. AIAA-2018-0167.
156. Zhu, Y.; Starikovskaia, S. Fast gas heating of nanosecond pulsed surface dielectric barrier discharge: Spatial distribution and fractional contribution from kinetics. *Plasma Sources Sci. Technol.* **2018**, *27*, 124007. [[CrossRef](#)]
157. Zhu, Y.; Wu, Y.; Wei, B.; Xu, H.; Liang, H.; Jia, M.; Song, H.; Li, Y. Nanosecond-pulsed dielectric barrier discharge-based plasma-assisted anti-icing: Modeling and mechanism analysis. *J. Phys. D Appl. Phys.* **2020**, *53*, 145205. [[CrossRef](#)]
158. Wei, B.; Wu, Y.; Liang, H.; Zhu, Y.; Chen, J.; Zhao, G.; Xu, H. SDBD based plasma anti-icing: A streamwise plasma heat knife configuration and criteria energy analysis. *Int. J. Heat Mass Transf.* **2019**, *138*, 163–172. [[CrossRef](#)]
159. Wei, B.; Wu, Y.; Liang, H.; Chen, J.; Zhao, G.; Tian, M.; Xu, H. Performance and mechanism analysis of nanosecond pulsed surface dielectric barrier discharge based plasma deicer. *Phys. Fluids* **2019**, *31*, 091701. [[CrossRef](#)]
160. Niu, J.J.; Sang, W.M.; Zhou, F.; Li, D. Numerical investigation of an anti-icing method on airfoil based on the NSDBD plasma actuator. *Aircr. Eng. Aerosp. Technol.* **2021**, *93/4*, 592–606. [[CrossRef](#)]
161. Gao, X.L. Development of High-frequency ns-SDBD Plasma Generator and Preliminary Study on Anti-Icing Experiment. Master's Thesis, Chongqing University, Chongqing, China, 2021. (In Chinese).
162. Liu, Y.; Kolbakir, C.; Starikovskiy, A.Y.; Miles, R.; Hu, H. An experimental study on the thermal characteristics of NS-DBD plasma actuation and application for aircraft icing mitigation. *Plasma Sources Sci. Technol.* **2019**, *28*, 014001. [[CrossRef](#)]
163. Luo, Z.B.; Xia, Z.X. Advances in synthetic jet technology and applications in flow control. *Adv. Mech.* **2005**, *35*, 220–234. (In Chinese)
164. Smith, B.L.; Glezer, A. The formation and evolution of synthetic jets. *Phys. Fluids* **1998**, *10*, 2281–2297. [[CrossRef](#)]
165. Nagappan, N.; Golubev, V.V. On Icing Control Using Thermally Activated Synthetic Jets. In Proceedings of the 51st AIAA Aerospace Sciences Meeting including the New Horizons Forum and Aerospace Exposition, Grapevine, TX, USA, 7–10 January 2013.
166. Nagappan, N.; Golubev, V.V. Parametric Analysis of Icing Control Using Synthetic Jet Actuators. In Proceedings of the 21st AIAA Computational Fluid Dynamics Conference, San Diego, CA, USA, 24–27 June 2013.
167. Nagappan, N. Numerical Modeling of Anti-Icing Using an Array of Heated Synthetic Jets. Ph.D. Thesis, Embry-Riddle Aeronautical University, Daytona Beach, FL, USA, 2013.
168. Li, Y.J. Research on Airfoil Separate Flow Control and Airfoil Icing Control Using Dual Synthetic Jet Actuator. Master's Thesis, National University of Defense Technology, Changsha, China, 2015. (In Chinese).
169. Li, Y.J.; Luo, Z.B. An experimental investigation on the process of droplet icing/frosting and defrosting/deicing using dual synthetic jet. *J. Exp. Fluid Mech.* **2016**, *30*, 27–32. (In Chinese)
170. Jiang, H. Research on Anti-Icing/De-Icing Using the Heated Dual Synthetic Jet Technology. Master's Thesis, National University of Defense Technology, Changsha, China, 2017. (In Chinese).
171. Liu, X.C.; Liang, H.; Zong, H.H.; Xie, L.K.; Su, Z. Experimental investigation on de-icing by an array of impact rod-type plasma synthetic jets. *Plasma Sci. Technol.* **2023**, *25*, 035504. [[CrossRef](#)]
172. Gao, T.X.; Luo, Z.B.; Zhou, Y.; Yang, S.K. A novel de-icing strategy combining electric-heating with plasma synthetic jet actuator. *Proc. IMechE Part G J. Aerosp. Eng.* **2020**, *235*, 095441002094472. [[CrossRef](#)]

**Disclaimer/Publisher's Note:** The statements, opinions and data contained in all publications are solely those of the individual author(s) and contributor(s) and not of MDPI and/or the editor(s). MDPI and/or the editor(s) disclaim responsibility for any injury to people or property resulting from any ideas, methods, instructions or products referred to in the content.